https://ntrs.nasa.gov/search.jsp?R=19820007806 2020-03-21T09:54:34+00:00Z

NASA CR-~~166806~~
166763

TECHNICAL REPORT 1939

ORI

ANALYSIS OF METEOROLOGICAL LOCATION AND DATA COLLECTION SYSTEM CONCEPTS

FINAL REPORT

DECEMBER, 1931

PREPARED UNDER CONTRACT NAS5-26604
FOR NATIONAL AERONAUTICS AND SPACE ADMINISTRATION
GODDARD SPACE FLIGHT CENTER
GREENBELT, MARYLAND 20771

Technical Report Documentation Page

1. Report No.	2. Government Accession No.	3. Recipient's Catalog No.

4. Title and Subtitle
Analysis of Meteorological Satellite Location and Data Collection System Concepts

5. Report Date
December , 1981

6. Performing Organization Code

7. Author(s)
R. G. Wallace and D. L. Reed

8. Performing Organization Report No.
TR 1989

10. Work Unit No. (TRAIS)

9. Performing Organization Name and Address
ORI, Inc.
1400 Spring Street
Silver Spring, Maryland 20910

11. Contract or Grant No.
NAS5-26604

13. Type of Report and Period Covered
Final
3 June 1981 - 3 December 1981

12. Sponsoring Agency Name and Address
User Terminal and Location Systems Branch
Instrument Systems Division
NASA-Goddard Space Flight Center, Greenbelt, MD 20771
Technical Officer: R. E. Taylor

14. Sponsoring Agency Code
974

15. Supplementary Notes

16. Abstract

A satellite system has been proposed that employs a spaceborne RF interferometer to determine the location and velocity of data collection platforms attached to meteorological balloons. This Meteorological Advanced Location and Data Collection System (MALDCS) is intended to fly aboard a low polar orbiting satellite such as the TIROS-N. The flight instrument configuration includes antennas supported on long deployable booms. The studies reported examined two related aspects of this system :

- The platform location and velocity estimation errors introduced by the dynamic and thermal behavior of the antenna booms.
- The effects of the presence of the booms on the performance of the spacecraft's attitude control system, and the control system design considerations critical to stable operation.

To obtain useful numerical results, the physical parameters of the "Astromast" type of deployable boom were used in the dynamic and thermal boom analysis, and the TIROS-N system was assumed for the attitude control analysis. The studies resulted in a determination of velocity estimation error versus boom length. This showed that there was an optimum, minimum error, antenna separation distance.

The report also includes a description of the proposed MALDCS system, and a discussion of ambiguity resolution.

17. Key Words	18. Distribution Statement
Satellite Position Location Radiofrequency Interferometer Spacecraft Attitude Control Spacecraft Dynamics Deployable Booms	

19. Security Classif. (of this report)	20. Security Classif. (of this page)	21. No. of Pages	22. Price
Unclassified	Unclassified	94	NA

TECHNICAL REPORT 1989

ORI
Silver Spring, Maryland 20910

ANALYSIS OF METEOROLOGICAL LOCATION AND DATA COLLECTION SYSTEM CONCEPTS

FINAL REPORT

DECEMBER, 1981

PREPARED UNDER CONTRACT NAS5-26604
FOR
NATIONAL AERONAUTICS AND SPACE ADMINISTRATION
GODDARD SPACE FLIGHT CENTER
GREENBELT, MARYLAND 20771

TABLE OF CONTENTS

I. INTRODUCTION AND SUMMARY

This report presents results of an investigation into a set of problems associated with designing and operating a long-baseline interferometer on a low-orbiting satellite for location and velocity estimation of data collection platforms. Previous studies [1] have shown that, with combined Doppler-interferometer processing, baseline lengths on the order of 30-50 m are needed to obtain platform velocity estimates accurate to within about 1 m/s during a single satellite overpass. This accuracy was deemed as necessary to support future meteorological balloon-tracking missions. The question addressed was whether dynamic and thermal movements of the boom(s) comprising the baseline would introduce errors so large that this accuracy could not be achieved.

The study effort also included an analysis of position estimate ambiguity resolution and the preparation of a system description. The outcomes of these tasks are included as appendices to this report.

1.1 PROBLEM STATEMENT

The assumed spacecraft configuration was that shown in Figure 1.1, consisting of a compact, massive spacecraft carring the interferometer antennas on one or two relatively light, stiff booms. The problems examined involved the behavior of the boom structure used to support the antennas. Accurate knowledge of the antenna locations is essential to accurate platform position and velocity estimation using an interferometer. If the attitude determination

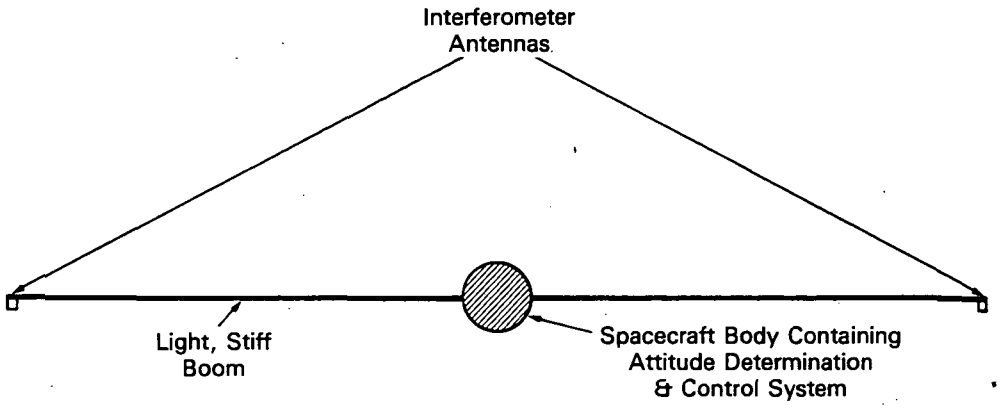

ALTERNATE CONFIGURATION:

FIGURE 1.1
ASSUMED SPACECRAFT CONFIGURATION

system contained in the spacecraft body is used to obtain the the antenna positions, then any unknown displacements of the antennas due to boom flexure or expansion/contraction will introduce errors in the platform location and velocity estimates. The booms are not perfectly rigid, and they will flex due to the small adjusting torques imparted to the spacecraft by the attitude control system. The booms are also not perfectly dimensionally stable, and they will bend and change in length in the face of varying sun illumination and earth albedo. One of the problem areas examined in this study was the unknown antenna displacements due to dynamic and thermal causes, and their impact on location and velocity estimation error.

The second potential source of problems examined was the effect that the long booms would have on the design and performance of the spacecraft's attitude control system. The booms, although their mass is a small fraction of that of the spacecraft, have a very large moment of inertia. In addition,

the booms have vibrational resonances. These two properties in combination can have a profound effect on the dynamics of the spacecraft as seen by the attitude control system. This area of investigation was in part motivated by the desire to build and fly a long baseline interferometer in the near term. Considering the current fiscal climate, the only feasible way of accomplishing this is to place the instrument on board a host spacecraft with other missions. (The NOAA TIROS-N spacecraft appears to be the only feasible vehicle for the interferometer.) Given that the interferometer must be accommodated by a spacecraft that has already been designed, it is necessary to investigate what dynamic properties the existing attitude control system design can tolerate. Further, if the existing design is found to be inadequate, it is necessary to determine if and how it can be modified to accommodate the interferometer.

1.2 SUMMARY OF STUDY

Available deployable boom designs were examined and one was selected as the best candidate based on mechanical characteristics and flight experience. The mass and stiffness parameters of the selected boom type ("Astromast," manufactured by Astro Research Corporation) were used in the subsequent analysis to obtain numerical results.

The problem was simplified by considering spacecraft rotations about only one axis. The equation of motion for a stiff boom attached to the spacecraft was solved with appropriate boundary conditions to obtain an effective moment of inertia for the spacecraft/boom system in response to a sinusoidal applied torque. (The effective moment of inertia is defined as the magnitude of the applied torque divided by the magnitude of the angular acceleration.) A transfer function giving the deflection amplitude of the boom endpoint for an applied sinusoidal torque was also determined. Both of these quantities are functions of the frequency of the applied torque, as well as boom mass, stiffness, and length. The effective moment of inertia was introduced into the spacecraft attitude control system equations to see the effects of the boom on system stability and determine how to compnesate for the effects. The transfer function was used to obtain the variance of the random dynamic antenna displacements by combining it with the estimated power spectral density of the torque applied by the attitude control system. The

antenna displacement variance was determined in this way for a range of boom lengths. The displacements due to thermal causes were also estimated, and both were introduced into the interferometer location and velocity estimation error model to find the effects on performance.

Without considering the antenna displacements, location and velocity error decreases with interferometer baseline (and boom) length. On the other hand, the magnitude of the displacements, and the errors they produce, increase with boom length. By combining the antenna displacement errors with errors from all other sources, it was anticipated that an optimum boom length could be found, giving a minimum combined error.

The attitude control system considered was that of the TIROS-N spacecraft. This was selected because it appeared to be the most likely host spacecraft. Although the parameter values used were peculiar to the TIROS-N, the methods of analysis used may be applied to other spacecraft as well because the control system of the TIROS-N is typical of those used on low-orbiting Earth-sensing spacecraft.

1.3 SUMMARY OF RESULTS

The analysis has shown that the unknown antenna excursions due to the thermal and dynamic flexures of an interferometer's boom structure will not introduce intolerable errors in velocity and position estimation, provided the spacecraft attitude control system has been compensated for the boom. Compensation consists of increasing the torque capabilities of the reaction wheel motors and installing a boom resonance filter. If we assume that the control system compensation restores the attitude control system response to what it is without the boom(s), the magnitude of the antenna deflection due to control system noise increases approximately as the fifth power of the length. The velocity and position estimation error decreases with baseline length and increases with antenna deflection, so there is an optimum length that gives the minimum error. Assuming reasonable values of phase and frequency measurement error, the optimum baseline length for velocity estimation is about 25 m for a single-boom system, and the velocity error standard deviation is about 1.8 m/s. Slightly smaller velocity error is obtained with two booms and a

longer baseline, but the error reduction does not make the added length worthwhile.

The results obtained depend critically on the Q of the booms used and the effectiveness of filtering to ensure attitude control system stability. Further investigation of these aspects is needed to provide more confidence in the results. As a check on the validity of the techniques used and the approximations made in the analysis, the entire coupled boom/spacecraft/attitude control system should be numerically simulated using a computer. This will reveal the transient behavior of the booms, as well as confirm the steady state performance. A transient analysis will make it possible to examine the effects of using the attitude control jets, and of large corrections due to computation errors or malfunctions.

II. DEPLOYABLE BOOM CHARACTERISTICS AND ANALYSIS

2.1 BOOM SELECTION

A number of different types of boom structures have been designed, constructed, and flown on spacecraft. ORI prepared a survey of the characteristics of the types of booms available [2] as part of another study. This survey, along with subsequent research, was the basis of the selection of a boom design for the long baseline interferometer.

The desired boom characteristics for this application are high stiffness, low mass, compactness in the undeployed state, ease of deployment, and good thermal stability. The kind with the best combination of these qualities of the available designs was the "Astromast," manufactured by Astro Research Corporation. This boom is constructed of three longerons held in an equilateral triangular cross section by stiff cross members and diagonal tension members. Two types, with different longeron design, are available. In the first type, the longerons are made up of jointed sections. The second type, which was the type selected, has continuous longerons (See Figure 2.1).

In its undeployed state, the three longeron rods are coiled into a helix having a length of about one-fiftieth of the deployed length. Because the coiled boom has stored energy, it tends to uncoil when freed, and deployment consists simply of releasing the coil. A lanyard can be attached to the end of the beam and payed out slowly to control the deployment. The deployment mechanism therefore consumes no power.

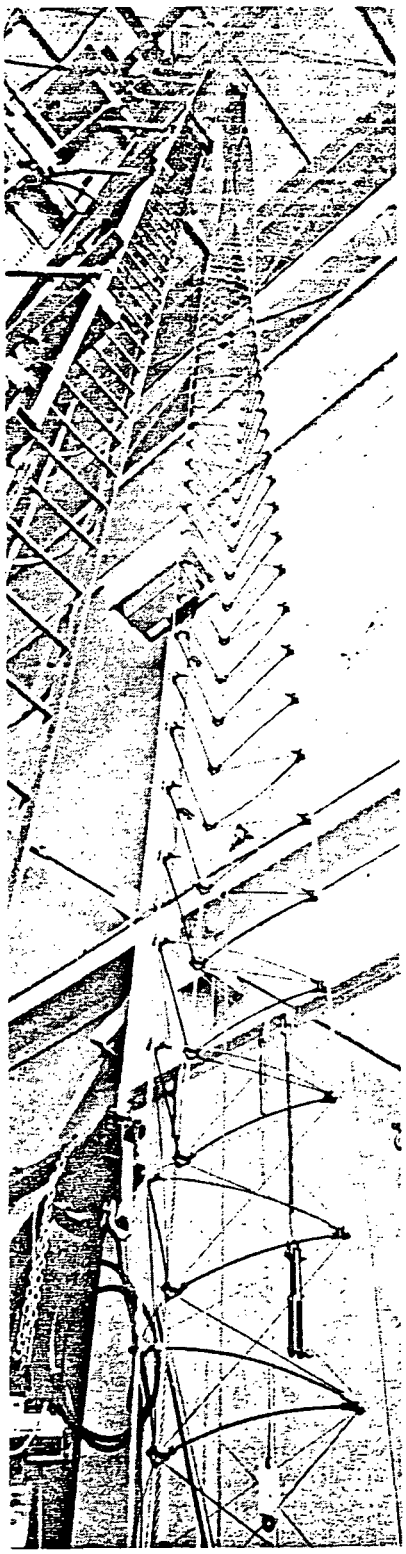

FIGURE 2.1. CONTINUOUS LONGERON ASTROMAST

Thermal flexing and twisting are minimized with this type of boom by constructing it in such a way that there is a slight residual twist left in it after it is fully deployed. The twist distributes the thermal stresses along the boom so that they tend to cancel out, resulting in little net bending or twisting. The twist also prevents the shadow of one longeron from falling on the full length of another, which would result in a drastic contraction of the shadowed member, and bend the boom.

2.2 BOOM PARAMETERS

The fiberglass continuous longeron Astromast boom can be constructed in any length and a wide range of diameters. (The diameter is actually the diameter of the circle enclosing the equilateral triangle cross section.) Two properties of the boom that are of interest, the mass per unit length and the bending stiffness, are determined solely by the diameter. Figure 2.2 gives these parameters as a function of diameter [3].

The stiffness and lineal mass of the boom are actually determined primarily by the diameter of the longerons and the material of which they are made. However, the longeron diameter is dependent on the boom diameter because of the requirement that it be capable of being coiled. The longeron diameter chosen is the largest that can be reliably coiled, without permanent deformation, into a helix having the boom's diameter. For fiberglass, the diameter of the longerons is made about 1.5 percent of the diameter of the boom.

Another parameter that is needed in the analysis that follows is an indication of the rate of damping of oscillations set up in the boom. This is a measure of how fast the energy of oscillation is transformed into heating of the boom, and is a complicated function of the material and construction of the boom. Damping rate is normally specified by either the logarithmic decrement, or the Q. Both terms involve the natural frequency of oscillation of the boom, so they are functions of boom length. Ideally, when a boom is caused to vibrate and then let free, the amplitude of the oscillations decay exponentially. If the time constant of the exponential decay is τ, the logarithmic decrement is defined as T/τ where T is the period of oscillation. The logarithmic decrement is just the natural logarithm of the

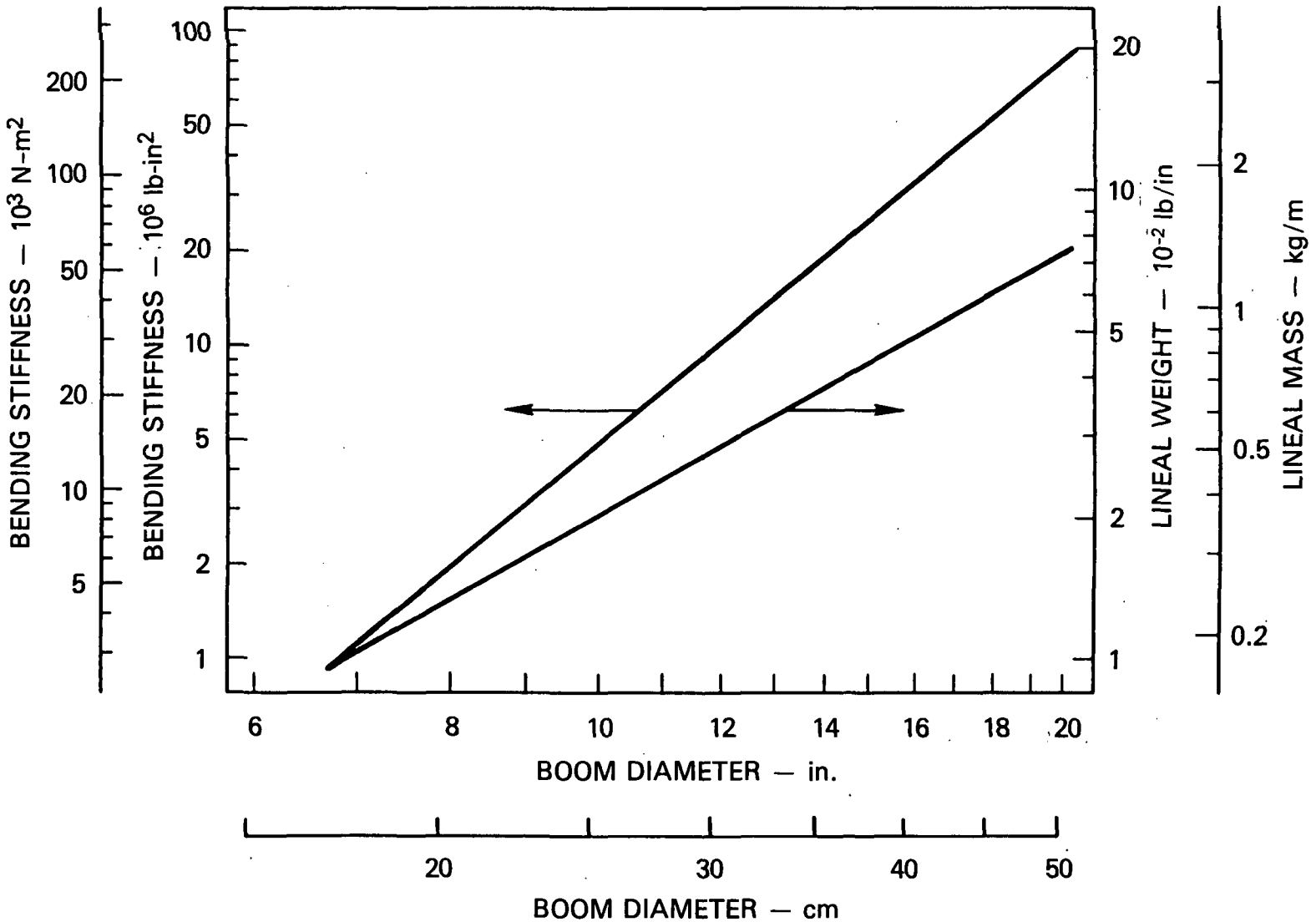

FIGURE 2.2. STIFFNESS AND LINEAL MASS FOR CONTINUOUS LONGERON ASTROMAST

ratio of the peak excursion values on successive cycles. The Q of the boom is defined as $\pi\tau/T$, or π times the reciprocal of the logarithmic decrement.

There is little data available indicating what the damping rate may be for booms of arbitrary diameter and length. Astro Research Corporation has supplied results from "twang" tests in which they recorded the excursions of vibrating booms on a strip chart and measured the logarithmic decrement. It was found that the logarithmic decrement decreased with amplitude, indicating that the damping is more complex than that of a simple exponential. However, since we are concerned here with very small deflections, we shall use the smallest values measured in the analysis. Astro Research gave the results of two tests, performed on booms of different length to diameter (L/D) ratios. On the basis of this, they estimated a logarithmic decrement for a third L/D ratio. Figure 2.3 shows the measured and estimated values. The plot shows that, in the judgement of Astro Research, the minimum logarithmic decrement varies inversely with L/D. The formula for Q implied by this is

$$Q \simeq 5\ (L/D)$$

Two more parameters are needed to describe the characteristics of the boom when it is twisted, rather than bent. These are the torsional stiffness and the torsional Q or logarithmic decrement. The minimum value of torsional Q was found by Astro Research to be about 200, independent of length, for nine inch diameter booms. The torsional stiffness is also available. Neither of these parameters were used in the analysis because torsional dynamics were not examined.

2.3 EQUATION OF MOTION AND BOUNDARY CONDITIONS

The dynamic properties of the boom will be found by solving a differential equation describing a stiff beam, subject to boundary conditions approximating that of a boom attached to a massive spacecraft. The equation will be solved assuming both a sinusoidal and a constant applied torque at the spacecraft center of mass. The constant-torque solution, which is analytical,

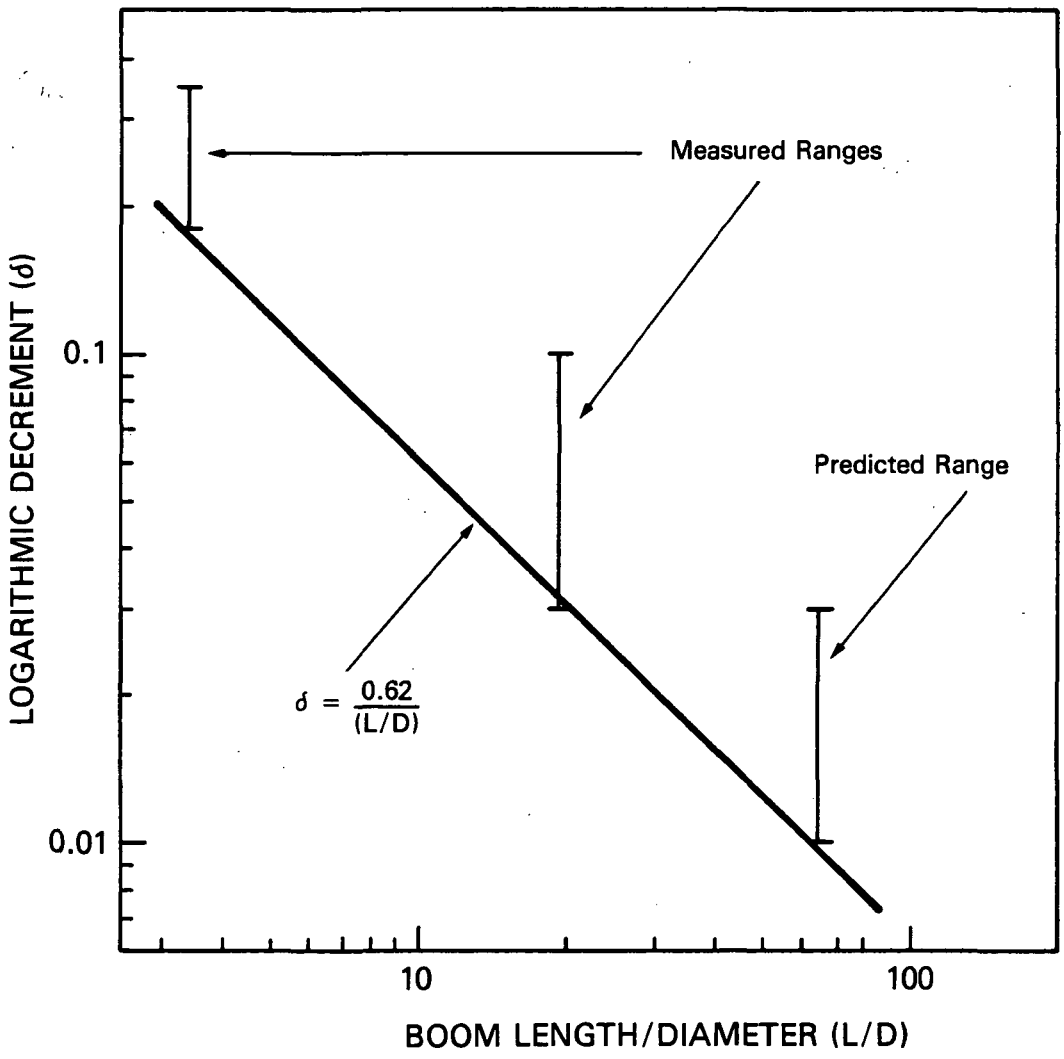

FIGURE 2.3. VALUES OF LOGARITHMIC DECREMENT FOR ASTROMAST

serves as a check on the sinusoidal-torque solution, which is numerical. At zero frequency, the sinusoidal solution should, and does, agree with the constant torque solution.

The boom/spacecraft model is shown in Figure 2.4. The spacecraft is assumed to have negligible dimensions compared with the boom, so it is modelled by a point mass with a specified moment of inertia, I_s, about its center of mass. The spacecraft is much more massive than the boom, so its center of mass is taken to be the center of rotation of the system. The boom extends along the x-axis and its deflections, which are assumed small, are in the y-direction. The angle of rotation of the spacecraft, also small, is taken to be equal to dy/dx at x=0. The boom length is L, and there is a mass m (the antenna) at its end point. Because the size and mass of the antennas is small compared to the boom, the antenna is assumed to have negligible moment of inertia. The boom is characterized by

ρ = lineal mass (kilograms/meter)

k = bending stiffness (Newton-meter-second^2)

The differential equation governing the shape of the boom as a function of time, y(x,t), is [4].

$$\frac{\partial^4 y}{\partial x^4} = -\frac{\rho}{k}\frac{\partial^2 y}{\partial t^2}$$

Boundary conditions account for shear forces and moments applied to the ends of the boom. If a force F were applied at x=0, we would have

$$-k\left.\frac{\partial^2 y}{\partial x^2}\right|_{x=0} = F$$

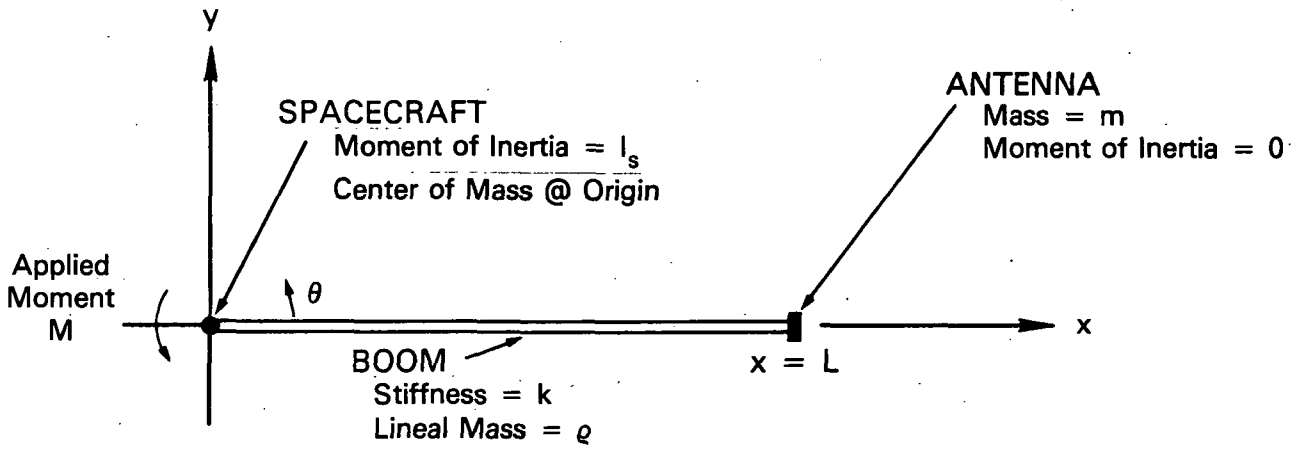

FIGURE 2.4. BOOM/SPACECRAFT MODEL

If a moment M were applied, then

$$-k \left.\frac{\partial^3 y}{\partial x^3}\right|_{x=0} = M$$

And similarly for x=L. The boundary conditions implied by the model so far are

Center of Mass is fixed: $Y(0) = 0$

Antenna produces no moments: $$-k \left.\frac{\partial^3 y}{\partial x^3}\right|_{x=L} = 0$$

Antenna produces a force equal to its mass times acceleration: $$m \left.\frac{\partial^2 y}{\partial t^2}\right|_{x=L} = k \left.\frac{\partial^3 y}{\partial x^3}\right|_{x=L}$$

Now if a moment M is applied at the spacecraft center of mass (x=0), we have a fourth boundary condition:

$$M = I_s \frac{\partial^2}{\partial t^2}\left(\left.\frac{\partial y}{\partial x}\right|_{x=0}\right) - k \left.\frac{\partial^2 y}{\partial x^2}\right|_{x=0}$$

The first term on the right-hand side is the spacecraft moment of inertia times its angular acceleration.

Note that there is no allowance for a damping factor in the equation. Damping has been left out to simplify the problem. It will be accounted for later by modifying the solutions obtained.

2.4 SINUSOIDAL SOLUTION

Since the differential equation is linear, we can assume a sinusoidal applied moment with radian frequency ω:

$$M = M_o e^{j\omega t}$$

and be assured that the solution is likewise sinusoidal with time:

$$y(x,t) = Y(x)\, e^{j\omega t}$$

The equation and boundary conditions for Y(x) now become

$$Y''''(x) = (\omega^2 \rho / k)\, Y(x)$$

$$Y(0) = 0$$

$$Y''(L) = 0$$

$$-m\omega^2 Y = kY'''(L)$$

$$M_o = -I_s \omega^2 Y'(0) - kY''(0)$$

where the primes denote differentiation with respect to x. The solution to the equation is

$$Y(x) = A \cosh\mu x + B \sinh\mu x + C \cos\mu x + D \sin\mu x$$

where

$$\mu = (\rho/k)^{1/4}\sqrt{\omega}$$

Using this in the boundary conditions results in four linear equations in four unknowns. It is possible to solve the equations for A, B, C, and D, which are functions of ω, k, ρ, m, M_o, and L. However, obtaining the analytical solution is extremely tedious and was not attempted. Instead, a computer was used to solve the equations for given values of the parameters. Some solutions are shown in Figure 2.5.

2.5 DERIVED FUNCTIONS

The solution for Y(x) is of little use in the problem at hand. What is needed instead are functions describing how the boom "feels" to the attitude control system, and how the endpoint (antenna) excursions are related to the applied moment. Both of these functions are derived from the solutions Y(x).

The attitude control system applies moments to the spacecraft through its momentum wheels and senses angular motions in response to those moments. The response is governed by the spacecraft dynamics. Spacecraft dynamics may be described as follows. Assume that the applied moment is sinusoidal, of magnitude M_o and radian frequency ω. (Of course, the applied moment never is sinusoidal, but assuming it is will allow us to later apply powerful spectral analysis techniques.) If the spacecraft were a rigid body with moment of inertia I_s, the response would be a sinusoidal angle variation with the same frequency, 180° out of phase, with magnitude θ_m given by

$$\theta_m = M_o\ (\omega^2 I_s)^{-1}$$

20 m Boom
20 in Diameter Astromast
5 lb Antenna

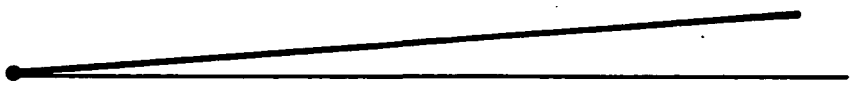

f = 0.16 Hz

f = 0.52 Hz
(First Resonance)

f = 0.95 Hz

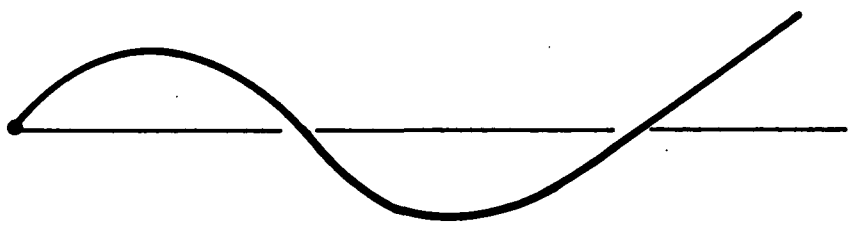

f = 6.37 Hz

FIGURE 2.5. SOME SOLUTIONS TO BOOM PROBLEM

Now if the spacecraft were not rigid (e.g., if it had a long boom attached), θ_m would not decrease smoothly with ω^2. Rather it would exhibit peaks and valleys as ω passed through the resonant frequencies of the boom. This behavior can be accounted for by replacing I_s in the equation with a function of ω:

$$\theta_m = M_o \left[\omega^2 I_{eff}(\omega)\right]^{-1}$$

The function $I_{eff}(\omega)$ will be called the effective moment of inertia. At zero frequency, corresponding to constant applied moment, $I_{eff} = I_s$.

I_{eff} is derived from the boom solution by writing

$$I_{eff}\,\theta = I_{eff}\,\frac{\partial^2}{\partial t^2}\left(\left.\frac{\partial y}{\partial x}\right|_{x=0}\right) = M_o\, e^{j\omega t}$$

which gives

$$I_{eff} = M_o(\omega^2\mu)^{-1}\ (B + D)^{-1}$$

where μ, B and D were given in the last section. Although M_o appears in the equation, B and D are proportional to M_o, so I_{eff} is independent of M_o.

The second derived function is the transfer function, $T(\omega)$, which is a measure of the amplitude of the antenna excursion per unit of applied moment. The value of Y(L) from the boom solution is the antenna excursion from the x-axis, but this is not the measure desired. A more meaningful quantity is the excursion from where the antenna would be if the boom did not bend. This is illustrated in Figure 2.6. We are interested in the error in determining the position of the antenna caused by unknown boom bending. The attitude determination system tells us where the antenna should be if there were no bending. This position is just L times the spacecraft attitude angle with respect to the x-axis. The error is the antenna's distance from this

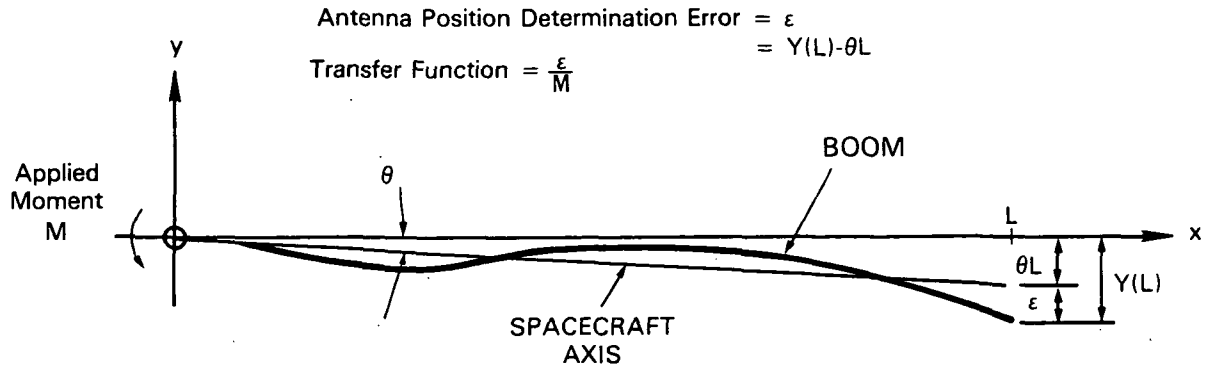

FIGURE 2.6. DEFINITION OF TRANSFER FUNCTION

ideal position, rather than its distance from the x-axis. The transfer function is therefore

$$T(\omega) = M_0^{-1} [Y(L) - L\theta]$$

$$= M_0^{-1} [Y(L) - LY'(0)]$$

Figures 2.7 through 2.10 show I_{eff} and T versus frequency for different boom lengths. The values used for k and ρ are those for a 10 and 20 inch diameter continuous longeron Astromast, and the value of I_s is 20,000 in-lb-s^2 (2256 N-m-s^2), the TIROS-N value. The antenna weighs 5 pounds.

Two resonance phenomena can be seen from the plots. The effective moment of inertia becomes infinite at the lowest resonance. At this point, the spacecraft's attitude is not changing, but the boom is still vibrating.

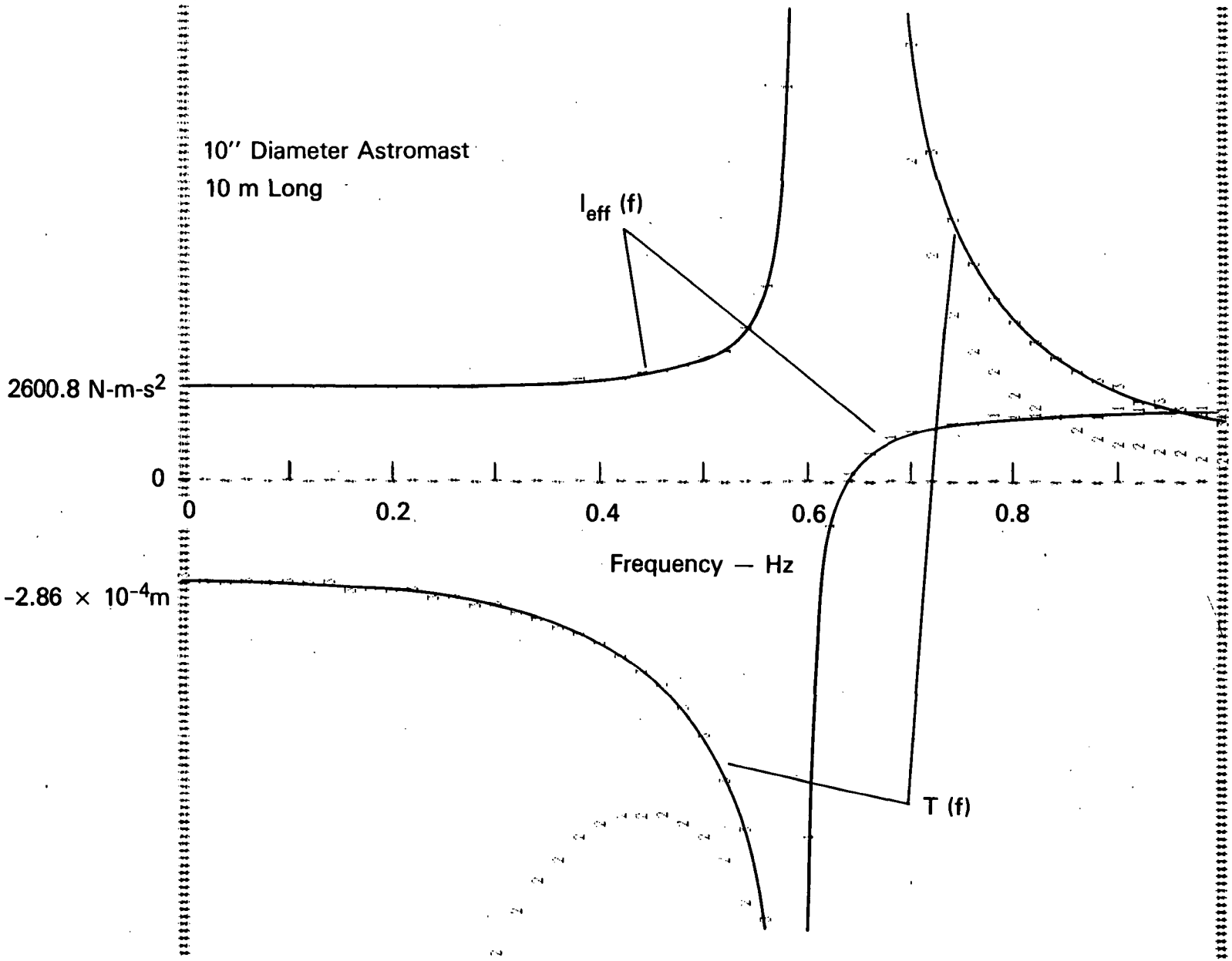

FIGURE 2.7. EFFECTIVE MOMENT OF INERTIA AND TRANSFER FUNCTION FOR 10-INCH ASTROMAST, 10 m LONG

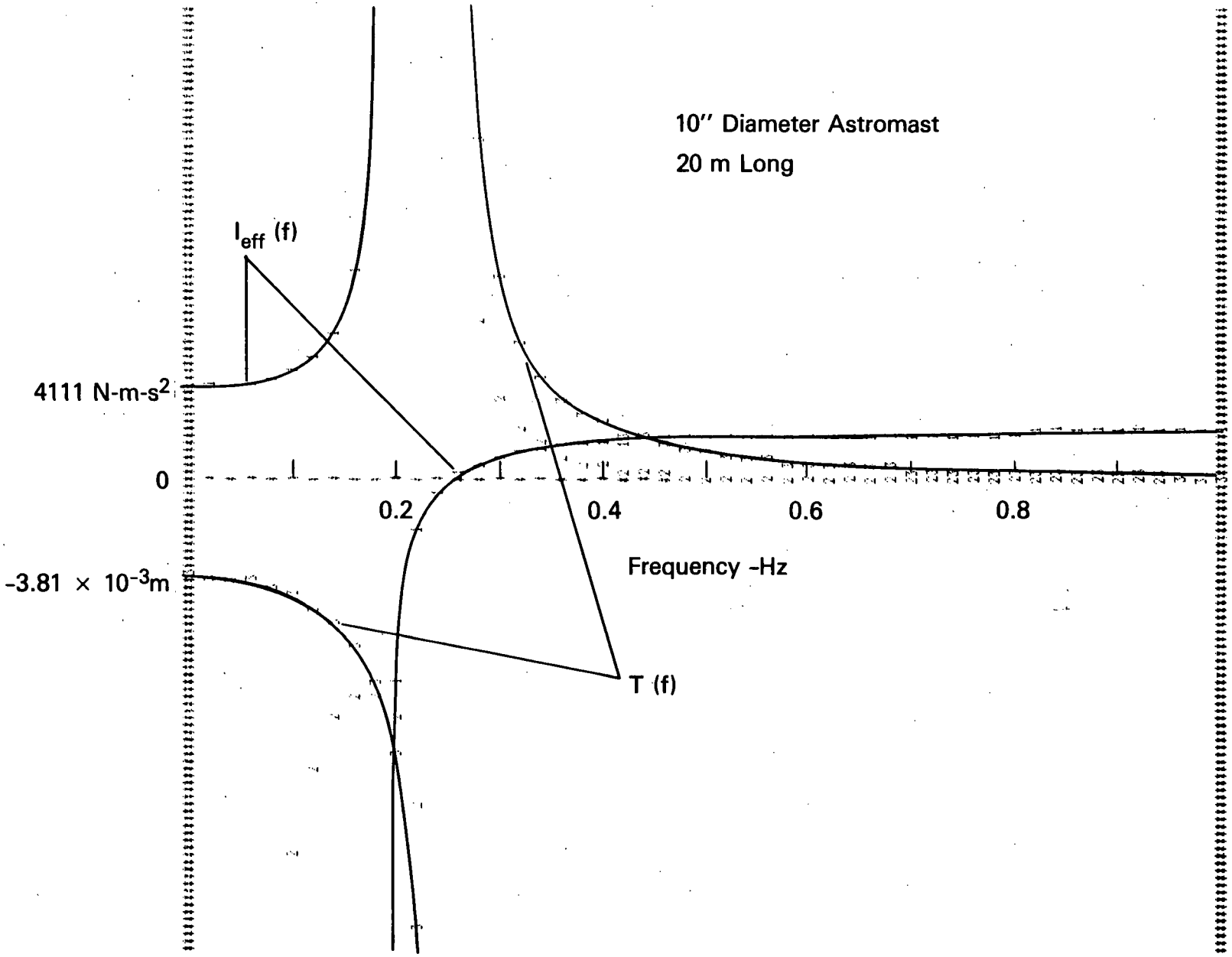

FIGURE 2.8. EFFECTIVE MOMENT OF INERTIA AND TRANSFER FUNCTION FOR 10-INCH ASTROMAST, 20 m LONG

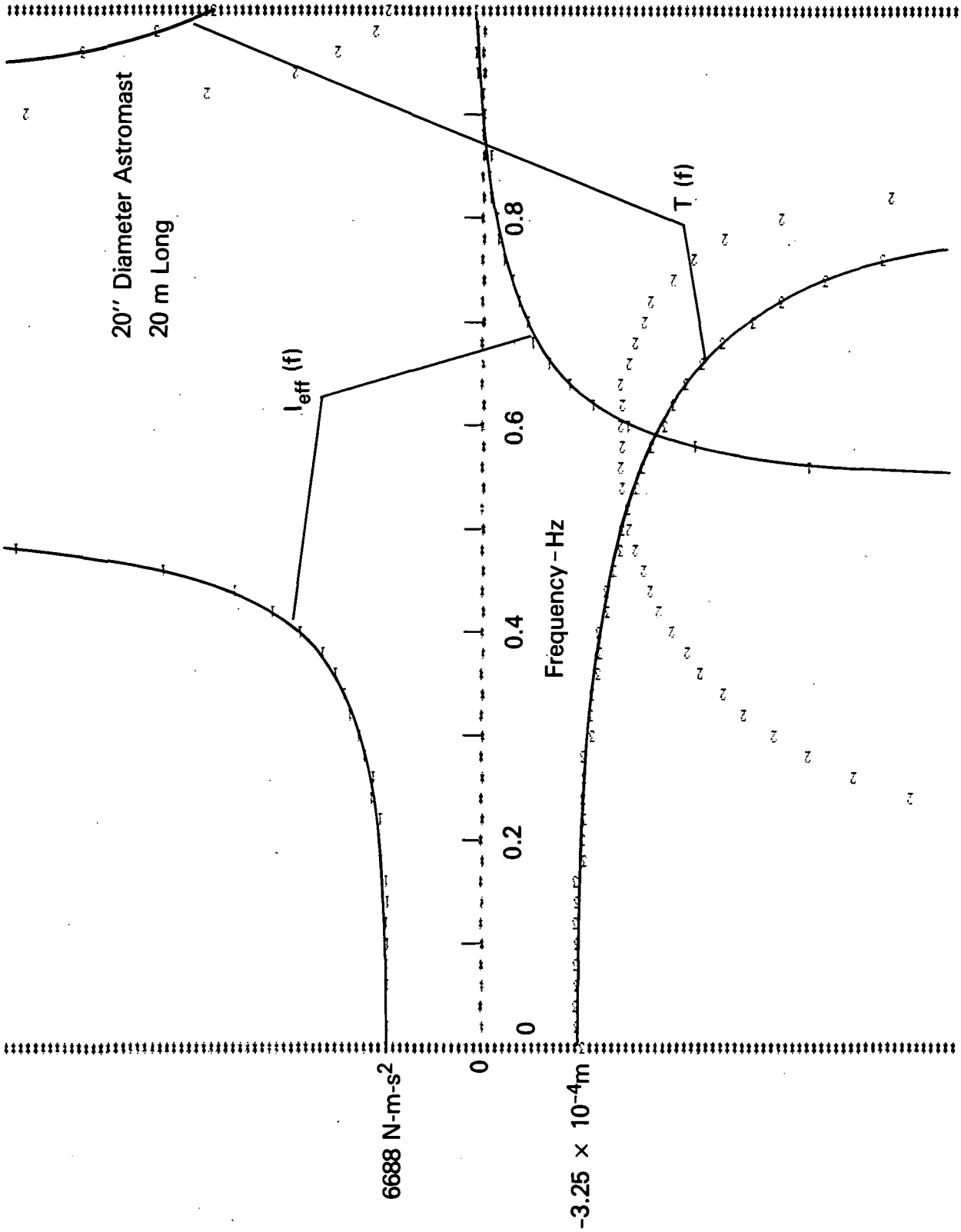

FIGURE 2.9. EFFECTIVE MOMENT OF INERTIA AND TRANSFER FUNCTION FOR 20-INCH ASTROMAST, 20 m LONG

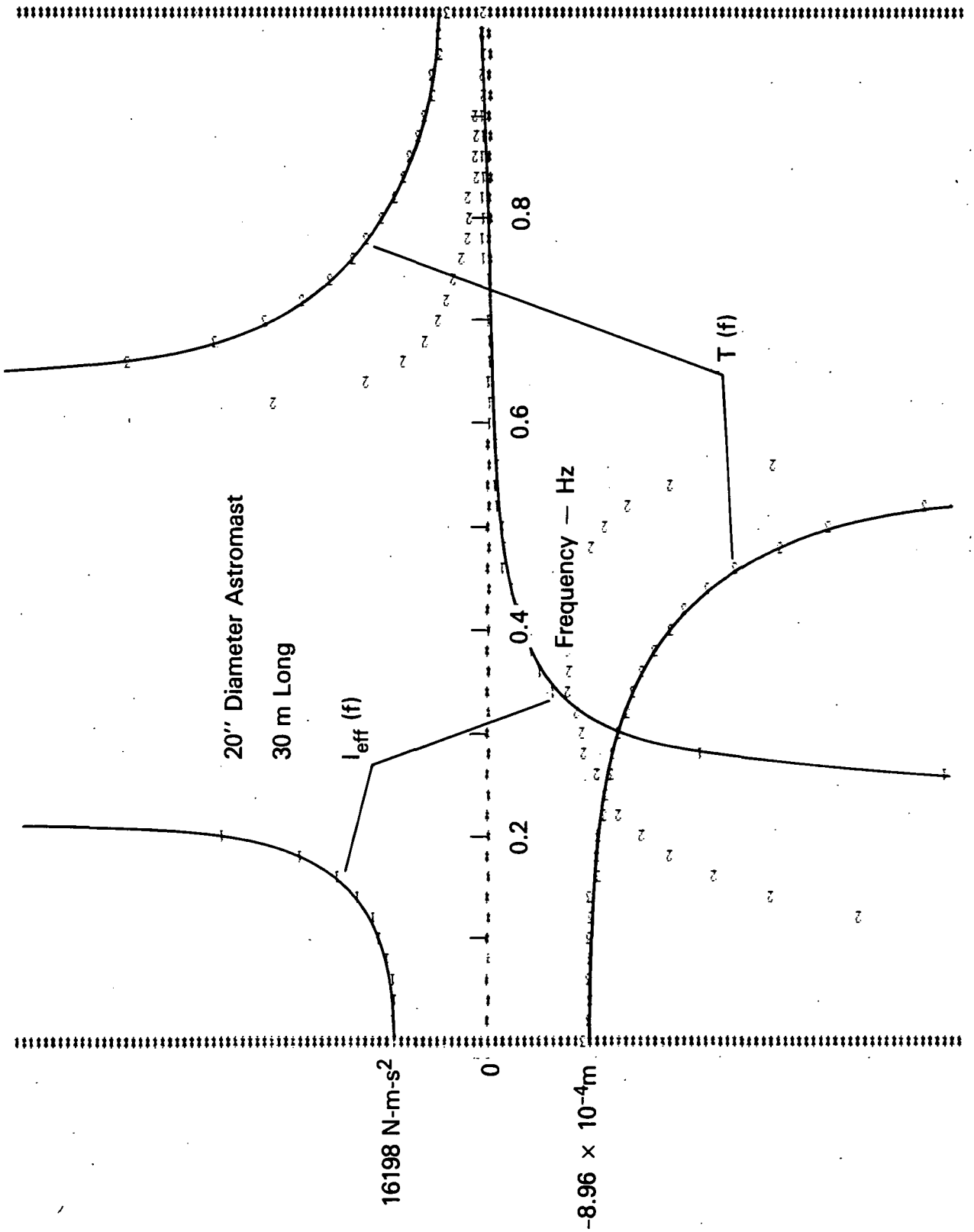

FIGURE 2.10. EFFECTIVE MOMENT OF INERTIA AND TRANSFER FUNCTION FOR 20-INCH ASTROMAST, 30 m LONG

At the higher frequency resonance, the magnitude of the boom vibration becomes infinite, and at the same time the effective moment of inertia becomes zero. The pair of resonances shown in each figure is actually the first of an infinite series of resonance, but the rest of them fall at frequencies greater than one Hz for the boom parameters selected in the figures. Figure 2.11 shows the frequencies of the transfer function resonances as a function of boom length and diameter.

Recall that no damping is included here. If it were, the quantities I_{eff} and T would be complex. Their amplitudes would have peaks instead of going to infinity, and their angles would change smoothly between 0 and 180° at the peaks. Also, the zero in I_{eff} would become a minimum.

2.6 THE CONSTANT-TORQUE SOLUTION

The shape of the boom and the end point displacement will now be found when the spacecraft is subjected to a constant torque. This will serve as a check on the computer-generated solution, since it corresponds to the sinusoidal solution at zero frequency. The constant-torque displacement might also be used as an upper bound on the dynamic displacement, by setting the torque value to the maximum amount that can be generated by the spacecraft's attitude control system. However, it is clear that this does not bound the displacement, because it does not consider the magnification effect of the boom resonances. The displacement can be made to exceed any bound, in theory, by even miniscule torques that are applied at the right frequency.

When the spacecraft/boom system is subjected to a constant torque, it must be turning with a constant angular acceleration, and this presents a small problem with the model. The boom model assumes that the boom displacement from the x-axis is small, but if the system is rotating the displacement must eventually become large. The problem is solved by considering the shape of the boom at the instant its attached end becomes parallel to the x-axis. At this instant, the y-acceleration of any point on the boom is equal to the angular acceleration times the point's distance from the origin, i.e.

$$\ddot{y} = x\ddot{\theta}$$

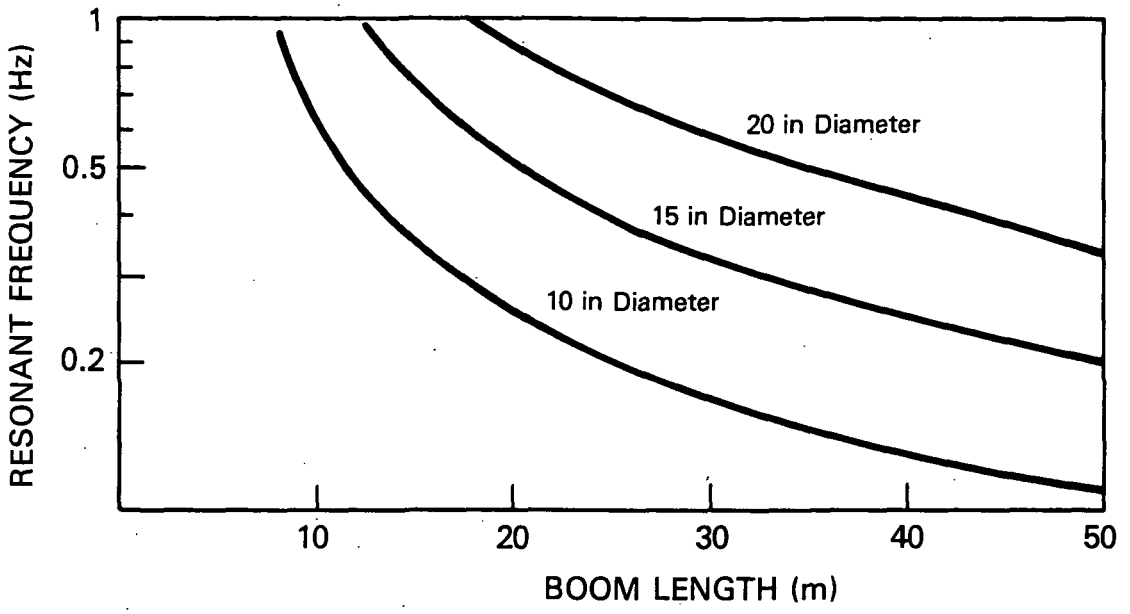

FIGURE 2.11. TRANSFER FUNCTION RESONANT FREQUENCY

But with a constant applied moment M,

$$\ddot{\theta} = M\,(I_b + I_s)^{-1}$$

where I_b and I_s are the boom and spacecraft moments of inertia, respectively. Using these in the differential equation for the boom, we have

$$y''''(x) = -(\rho/k)M(I_b+I_s)^{-1}x$$

The solution is

$$y = \rho M k^{-1}(I_b+I_s)^{-1}(A+Bx+Cx^2+Dx^3-x^5/5!)$$

The boundary conditions are

$$y(0) = 0$$
$$y'(0) = 0$$
$$y''(L) = 0$$
$$mML(I_b+I_s)^{-1} = ky'''(L)$$

Applying these yields y(x), which at the endpoint has the value

$$y(L) = -\rho Mk^{-1}(I_b+I_s)^{-1}[(11/120)L^5+(1/3)mL^4/\rho]$$

with

$$I_b = (1/3)\rho L^3+mL^2$$

Values of y(L) and I_b versus boom length and diameter are plotted in Figure 2.12. The zero-frequency values for T given in the last section agree with these.

2.7 THE ANALOGOUS SYSTEM

In later chapters, it will be necessary to have approximations to the boom response when the Q is finite, or damping is considered. These approximations will be derived from the solution to a problem that is analogous to the boom problem. The analogous system model allows damping to be considered, and provides an analytical solution. The transfer function and effective moment of inertia derived from the analogous system closely approximate those found for the boom when the Q is made infinite, and so provide a way of introducing damping into the boom dynamics.

The analogous dynamic system is shown in Figure 2.13. A mass is suspended from a spring at the end of a massless, perfectly stiff, boom that is attached to a massive spacecraft. The spacecraft is subjected to a sinusoidal moment, $M_o e^{j\omega t}$, at its center of mass. The equations governing the position of the end of the boom, y_2, and of the mass, y_1, are

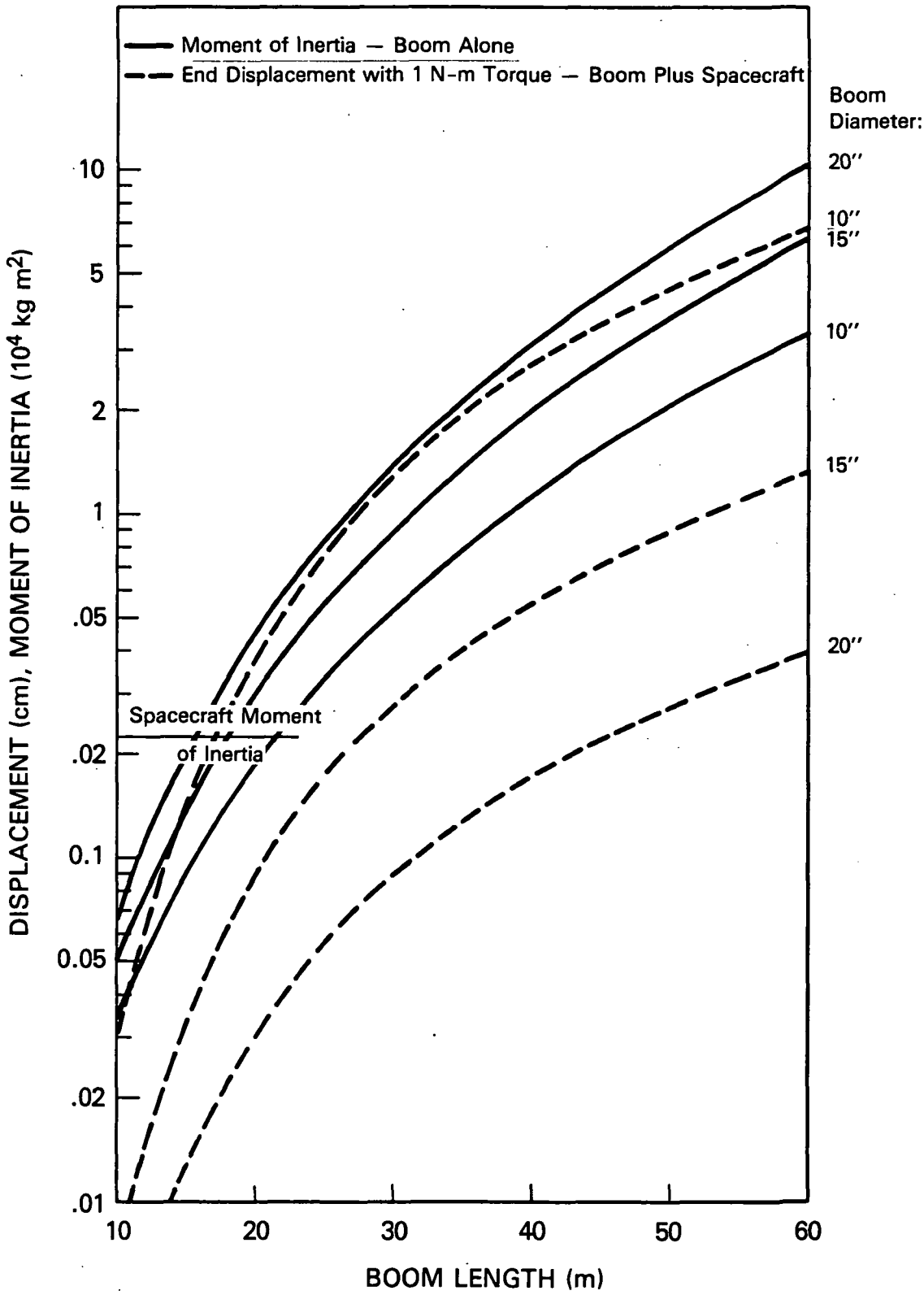

FIGURE 2.12. BOOM MOMENT OF INERTIA AND END DISPLACEMENT WITH CONSTANT 1 Nm TORQUE

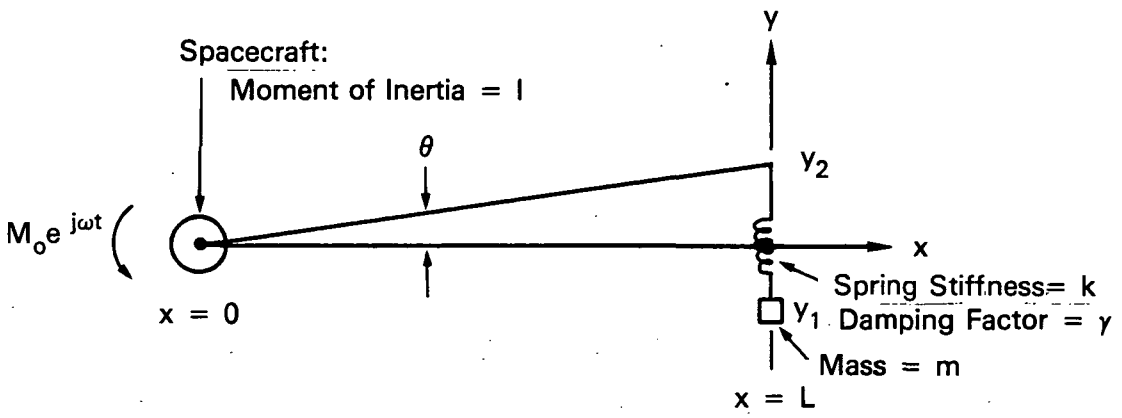

FIGURE 2.13. SPRING-MASS SYSTEM ANALOGOUS TO BOOM

$$m\ddot{y}_1 = k\,(y_2 - y_1) + \gamma(\dot{y}_2 - \dot{y}_1)$$

$$M_0 e^{j\omega t} = I\ddot{\theta} + Lk\,(y_2 - y_1)$$

$$y_2 = L\theta$$

It is assumed here that displacements are small so that $\sin\theta \simeq \theta$ and $\cos\theta \simeq 1$. The constant γ accounts for friction which converts the energy of motion into heat and damps the oscillations. The solution of these equations, which will be utilized in later chapters, is

$$y_2 - y_1 = e^{j\omega t}\,\frac{N_0 Lm}{(I + m\,L^2)(k + j\omega\gamma) - Im\omega^2}$$

$$\theta = e^{j\omega t}\,\frac{N_0(k + j\omega\gamma - m\omega^2)}{Im\omega^4 - (I + m\,L^2)(k + j\omega\gamma)\omega^2}$$

III. SPACECRAFT ATTITUDE CONTROL

A spacecraft with long flexible appendages, such as interferometer antenna booms, would have dynamic characteristics quite different from those of a rigid body. Because of this, an attitude control system designed for a rigid body spacecraft would not be expected to function as well with the appendages attached. The system might need some modification to accommodate the change to the spacecraft dynamics. While the presence of the booms will affect the attitude control system performance, the excitation of boom vibrations by the control system also affects interferometer location estimation performance. Thus, there is a mutual interaction between the interferometer and the attitude control system. In this chapter, one aspect of this interaction is discussed, and the parameters critical to the attitude control system performance are identified. Possible modifications of a particular system that are necessary to permit attitude control with booms attached are also discussed. In the next chapter, the platform location errors due to attitude control system/boom interaction are estimated, assuming that the attitude control system has been modified as required.

The attitude control system considered here is that of the TIROS-N spacecraft. This spacecraft has been selected because it is apparently the only viable candidate for a host for the interferometer instrument. However, the selection of this particular spacecraft for the analysis is not as restrictive as it may first appear. This is because the method of analysis used is applicable to any spacecraft with a similar attitude control system, and the TIROS-N system is typical of those used in low-orbiting, earth-sensing satellites.

3.1 TIROS-N ATTITUDE DETERMINATION AND CONTROL SYSTEM (ADACS)

The TIROS-N ADACS [5] uses an earth horizon sensor, a sun sensor, and gyros for attitude sensing, and momentum wheels and magnetic torquing coils for control. In addition, nitrogen thrusters are available for initial stabilization and emergencies. The infrared earth sensor provides attitude information about the pitch and roll axes, which are along the velocity vector and normal to the orbit plane, respectively. Yaw position information is provided by the yaw gyro, which is updated once per orbit by the sun sensor. The gyros provide roll, pitch and yaw rates. The positions and rates are sampled every half-second and the samples are used to calculate torque commands that are transmitted to the reaction wheel motors.

The torques applied by the motors are equal and opposite, on the average over an orbit, to the torques applied to the spacecraft by external forces. Gravity gradients, the solar array drive, and scanning instruments on board are the primary sources of external torque. The magnetic torque coils are energized at certain points in the orbit to "dump" the momentum built up in the reaction wheels as a result of these torques. In addition to these "secular" torques, the reaction wheels must also compensate for torques that are felt instantaneously, but average to zero over an orbit.

The torque generated by one of the reaction wheel motors is a linear function of the position, rate, and integral of position of the spacecraft about that wheel's axis. In the roll and pitch axes, the position and integral terms are provided by the earth sensor and the rate term comes directly from the gyro. In the yaw axis, all three terms are derived from the gyro. The block diagram of one axis of the system (either the pitch or roll axis) is shown in Figure 3.1 [6]. In the figure, "s" is used to indicate differentiation in the Laplace transform domain, and K_P, K_R, and K_I are the position, rate and integral term gains, respectively. The position and rate reference inputs shown in the figure are actually fictitious. They are shown to agree with the canonical control system block diagram, but may be neglected for the present, since they have zero value.

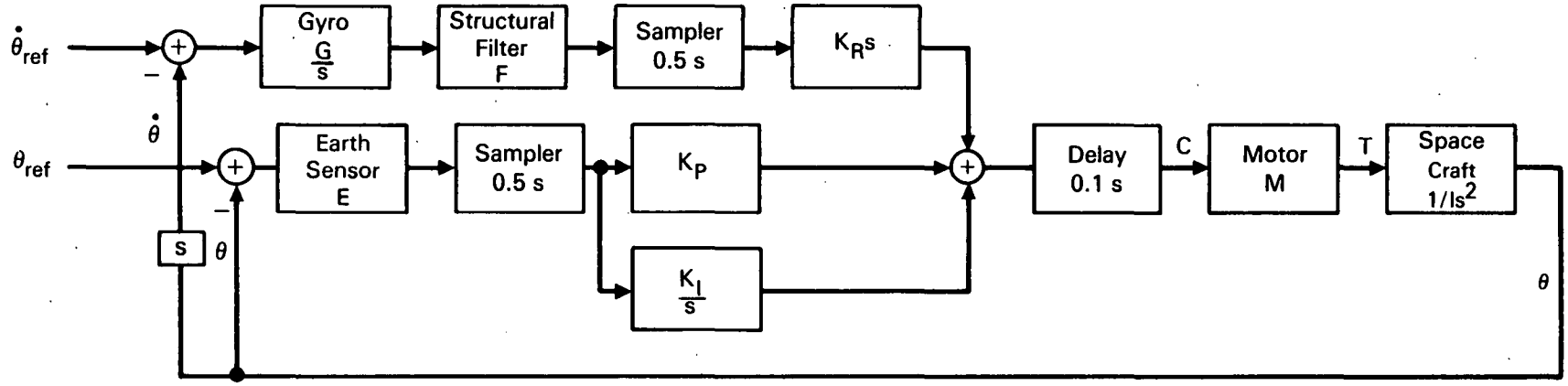

FIGURE 3.1. TIROS-N ATTITUDE CONTROL SYSTEM

Each block of the diagram has a known transfer function. The gyro is mainly an integrator of the angle rate, but its transfer function has in addition a pair of poles at $\sigma + j\omega = -8.88 \pm j\ 2\pi(1.74)$. The structural filter is apparently intended to filter out any high frequency structural responses. It is a low pass filter with a 0.6 Hz 3dB cut-off frequency. The output of the structural filter is sampled at 0.5 second intervals, and the differentiation and multiplication indicated by the "$K_R s$" block is performed digitally. The earth sensor contains a 0.4 second delay and a simple pole at $s = -1.67$, giving a corner frequency of 0.27 Hz. The earth sensor output is sampled at 0.5 second intervals, and the indicated multiplication, integration and summing are performed digitally. The 0.1 second delay accounts for the computation time. The sum of the rate, position, and integral terms is the command voltage C applied to the reaction wheel motor. The motor produces a torque proportional to the command voltage, which is applied to the spacecraft axis. The spacecraft's angular position, θ, is the second integral of the torque divided by the moment of inertia, I, as indicated by $1/Is^2$ in the diagram.

The loop gain of the system, H(s), is the total gain around the loop. For the system shown in Figure 3.1, we have

$$H(s) = MI^{-1}s^{-2}[GFK_R + E(K_P + K_I/s)]$$

The magnitude and phase of H(s) with $s=j2\pi f$ are shown in Figure 3.2. H(s) determines the stability of the system, as discussed in the next section.

3.2 STABILITY CONSIDERATIONS

It is easy to imagine how an attitude control system, if not properly designed, could become unstable when the vehicle it controls has dynamic resonances. If the delay in the response of the system were near the period of a natural resonance, the correcting torques could be applied at just the times necessary to reinforce the natural vibration. The magnitude of the vibration would grow and quickly get out of hand. An example of an attitude control system that became unstable in the presence of flexible booms is that of the first Polar Orbiting Geophysical Observatory (POGO) spacecraft. This early satellite used gas jets for attitude control. Because of stability

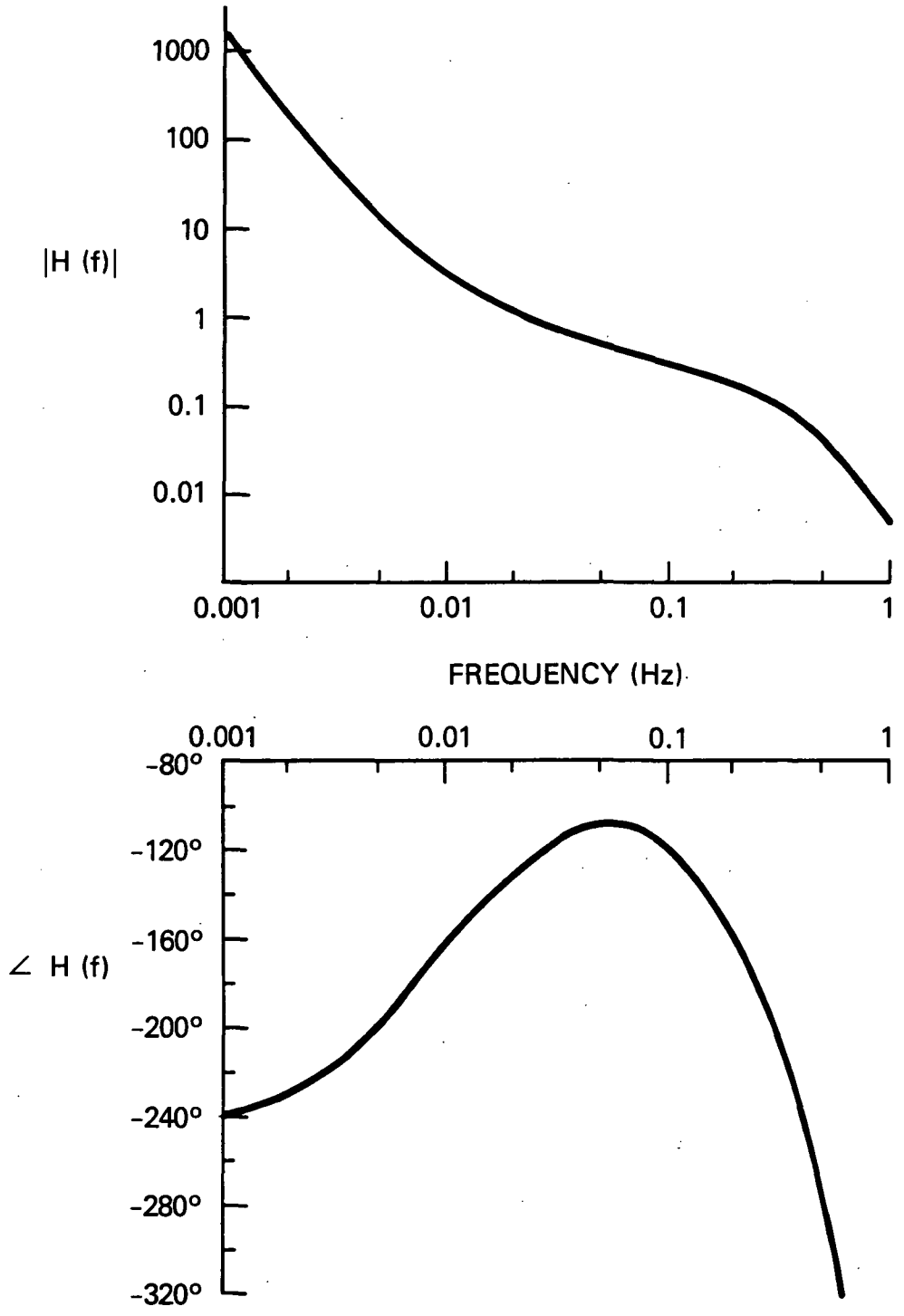

FIGURE 3.2. LOOP GAIN

problems, the entire lifetime supply of gas for the jets was used up in a matter of hours.

Here, the stability of a reaction wheel, rather than jet control system is addressed. Analysis of a jet control system is more difficult and requires knowledge of the transient response of the spacecraft and its appendages. The TIROS-N system includes jets as back-up to the reaction wheels, so the system stability using the jets will need to be studied eventually.

There are a number of criteria that can be used to tell whether or not a control system will be stable, and quantitatively how stable it will be. One of these, the Nyquist criterion, will be introduced below and then applied to the TIROS-N attitude control system. The Nyquist criterion will then be used to assess the system stability when a boom is included on the spacecraft. It will also be used to help arrive at system modifications that including the boom may require.

The Nyquist stability criterion [7] is based on a principle of complex variables, and is applied to the loop gain of the system, H(s). Complex variable theory states that any contour in the s-plane maps into a corresponding contour in the H(s) plane. The Nyquist criterion places requirements on the mapping onto the H(s) plane of a particular contour in the s-plane. That contour is shown in Figure 3.3. It consists of the $j\omega$ axis, a small semicircle of radius approaching zero about the origin, and a large semicircle of radius approaching infinity, taking in the right half-plane. The direction of this contour is counter-clockwise about the right half-plane. The Nyquist criterion states that for the system to be stable, the corresponding contour in the H(s)-plane must either not encircle the point $-1+j0$, or it must encircle that point in the clockwise direction. An encirclement in the counter-clockwise direction indicates that the system is unstable.

This criterion will now be applied to the TIROS-N attitude control system. If the magnitude and angle plots for H(f) of Figure 3.2 are replotted in polar coordinates, the solid line of Figure 3.4 is obtained. (Note that

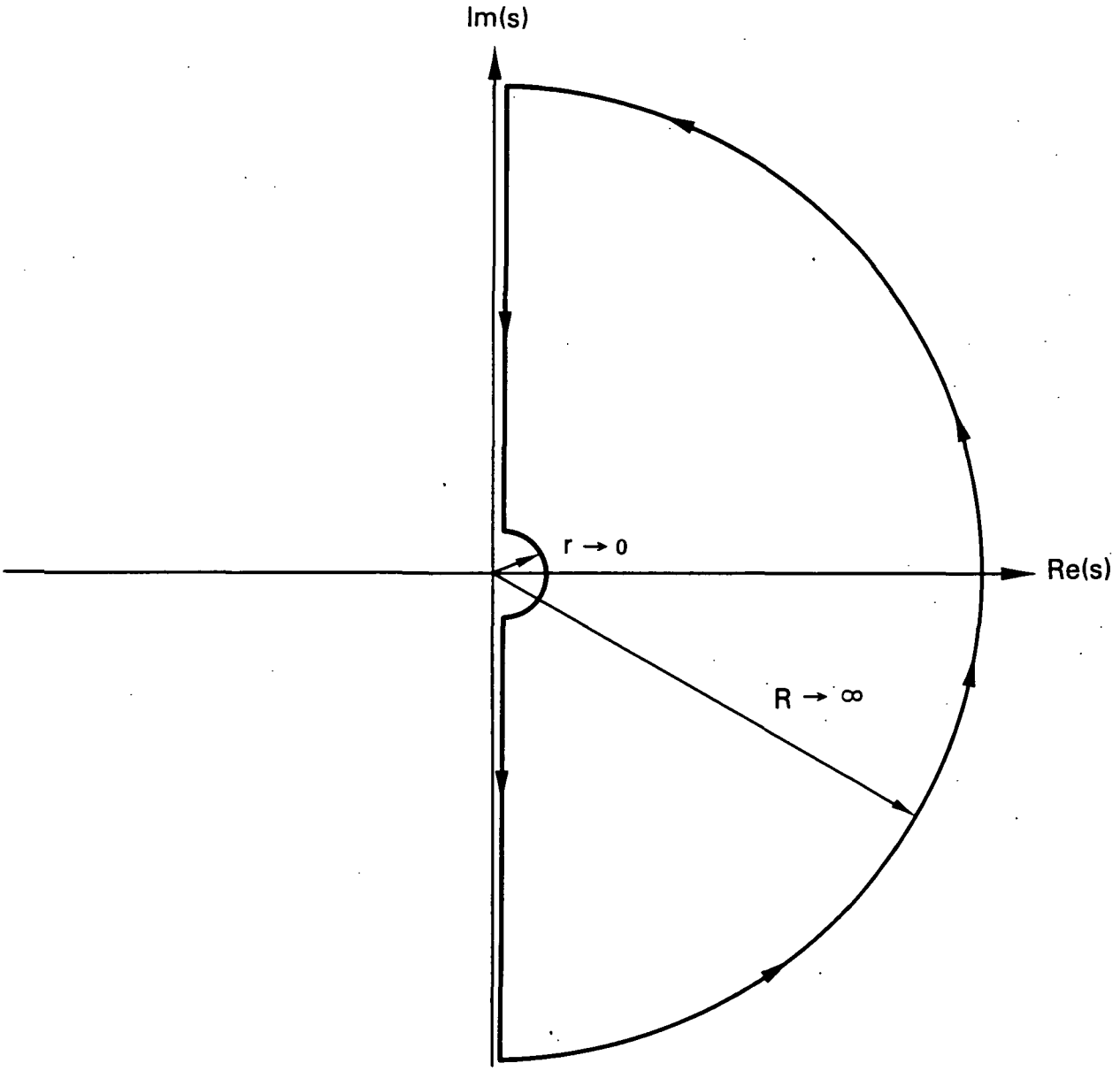

FIGURE 3.3. NYQUIST CRITERION CONTOUR IN THE s-PLANE

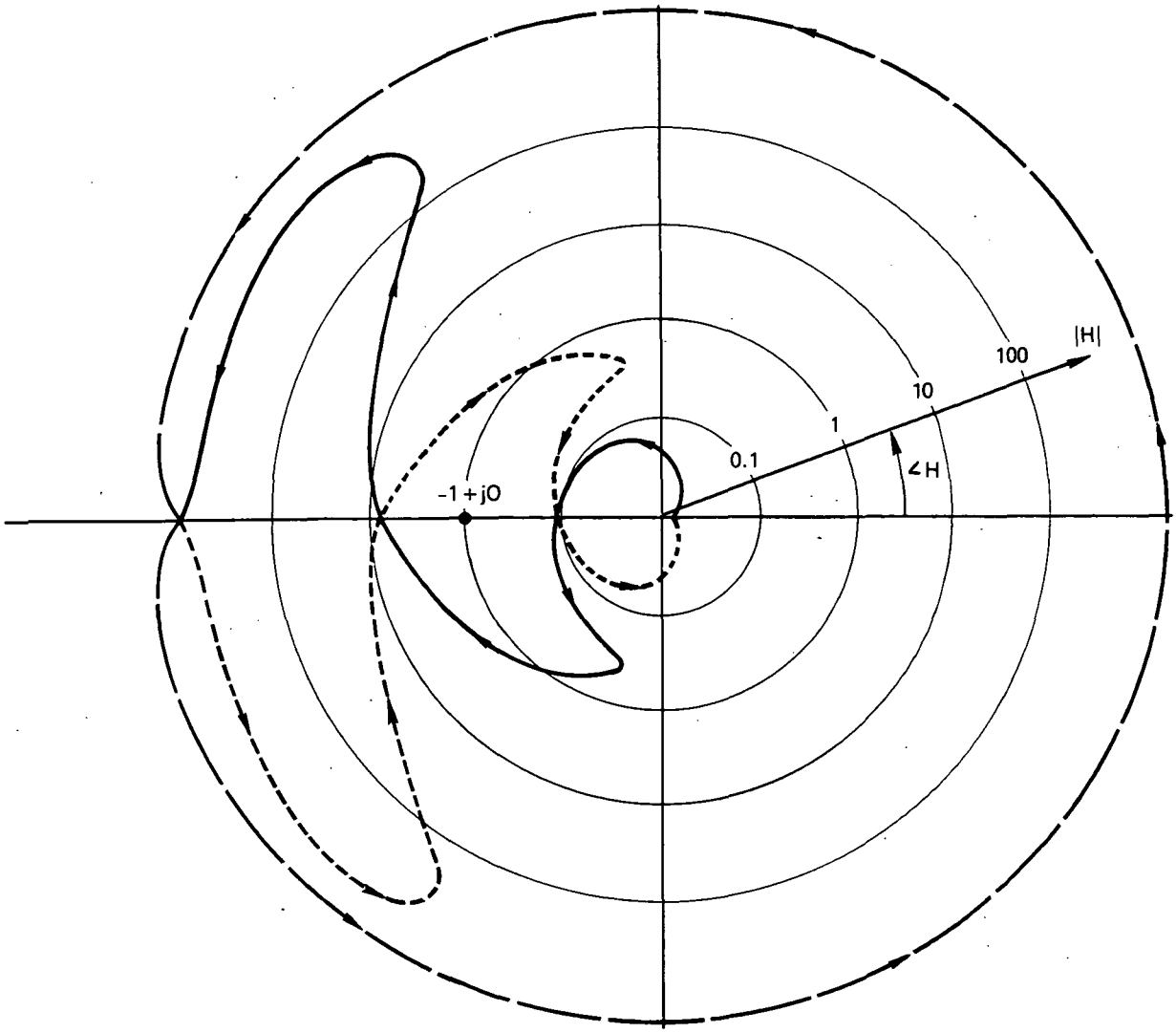

FIGURE 3.4. NYQUIST CRITERION CONTOUR IN THE H(s) PLANE

the radius coordinate in this figure is logarithmic.) This is the part of desired contour for positive values of ω ranging from infinity to a small value. (As ω becomes infinite the contour spirals into the origin.) The contour for negative values of ω ranging from a small value to minus infinity is just the mirror image of this, due to the mathematical characteristics of all realizable functions H(s). This part of the contour is shown dotted in the figure. The part of the contour corresponding to very small values of s, including the semicircle about the origin, is shown, approximately, as a dashed line. A pole in the motor transfer function with a corner frequency of about 3×10^{-4} Hz causes the angle of the loop gain to tend toward 180° as the frequency goes to zero. The contour in the s-plane includes a semicircle about the origin with a vanishingly small radius. The loop gain behaves approximately as $1/s^2$ at very small values of s, so as the angle of s makes an excursion of -180° about the origin, the angle of H(s) makes an excursion of +360°. The small clockwise semicircle therefore maps into a full counter-clockwise circle with very large radius, as shown in Figure 3.4. Examination of the contour in the figure shows that there is no encirclement of the -1+j0 point, so the system is stable. (This is hardly surprising.)

Two commonly-used measures of the degree of stability of a system are the gain margin and the phase margin. The gain margin is defined by

$$\text{Gain Margin (dB)} = -20 \log \left| H\,(180^\circ) \right|$$

where $\left| H(180^\circ) \right|$ denotes the loop gain magnitude when its angle is 180°. For the TIROS-N system, the gain margin is about 20 dB. The phase margin is the angle of the loop gain when its magnitude is 1, minus 180°. For the present case, the phase margin is about 50°. The gain and phase margins are indications of the amount of overshoot in the transient response, and the size of the resonant peak of the frequency response of the system. Both of these generally increase with decreasing gain and phase margin.

The 20 dB gain margin means that if the loop gain were increased by a factor of ten or more, the system would become unstable. This can be seen from the plot of the loop gain in Figure 3.4. Increasing the gain would cause the contour to expand radially. If the expansion were by a factor of ten or

more, the -1+j0 point would move to a location where it was encircled by the contour, indicating instability.

Instability can be induced in the system in another way besides increasing the loop gain beyond the gain margin. If the gain were reduced by a factor of 5 or more, the contour would be shrunken to the point where the -1+j0 point was encircled, again indicating instability. This system is therefore conditionally stable, meaning it becomes unstable when the magnitude of the loop gain is outside of a range of values.

3.3 EFFECTS OF BOOM ON ATTITUDE CONTROL SYSTEM PERFORMANCE

The effects on the control system operation of a boom attached to the spacecraft can now be estimated, using the above observations and the spring-mass approximation to the boom from Chapter 2.

From the standpoint of the attitude control system, attaching a boom to the spacecraft is accounted for by replacing the spacecraft moment of inertia in the control system block diagram, I_s, with the spacecraft/boom system effective moment of inertia, I_{eff}. I_s is nearly constant with frequency, at least in the frequency range of interest. But I_{eff} exhibits a resonance phenomenon at frequencies low enough to affect control system operation. As can be seen from the plots in Chapter 2, the general behavior of I_{eff} is as follows.

- At very low frequencies, I_{eff} equals the sum of the moments of inertia of the spacecraft and the boom.
- I_{eff} increases with frequency and reaches a peak at some frequency f_1, determined by boom parameters.
- I_{eff} decreases as the frequency is increased beyond f_1, and reaches a minimum at a higher frequency, f_2.
- At frequencies beyond f_2, I_{eff} increases and asymptotically approaches the moment of inertia of the spacecraft alone.

When no loss is present, the peaks are infinite and the minimum is a zero. The angle of I_{eff}, when no loss is present, is zero at frequencies below f_1 and greater than f_2, and 180° between f_1 and f_2.

More insight into the behavior of I_{eff} is obtained with the help of the analogous spring-mass problem presented in section 2.7. An effective moment of inertia can be defined for that model in exactly the same way as defined for the boom. It turns out to be the following

$$I_{eff} = I_s \frac{\omega^2 - \omega_2^2 - j\omega(\omega_2/Q)}{\omega^2 - \omega_1^2 - j\omega(\omega_1/\omega_2)(\omega_1/Q)}$$

where

$$\omega_1 = \sqrt{k/m}$$

$$\omega_2 = [k(m^{-1} + L^2/I_s)]^{1/2} > \omega_1$$

$$Q = k/(\gamma\omega_2)$$

Here Q is defined as in Chapter 2. This I_{eff}, when Q is infinite, has the same behavior as the corresponding function found for the spacecraft/boom system. We can therefore use it as an approximation to the spacecraft/boom system when loss is present.

Figure 3.5 shows I_{eff} from the above formula, plotted in magnitude and phase form and in polar form. The parameters used in calculating I_{eff} for the plot were chosen so that the asymptotic values and resonant frequencies were the same as those of the spacecraft/boom system of Figure 2.7. Values of Q used in Figure 3.5 are 10 and 20. These Q values were selected for illustrative purposes only; typical values for actual booms are on order of magnitude greater than this.

Figure 3.6 shows the effect of including the boom described by Figure 3.5 in the loop gain polar plot. Here, the loop gain without the boom (shown in Figure 3.4) has been multiplied by I_s/I_{eff}. This is the same as replacing I_s by I_{eff} in the loop gain expression. It has the effect of

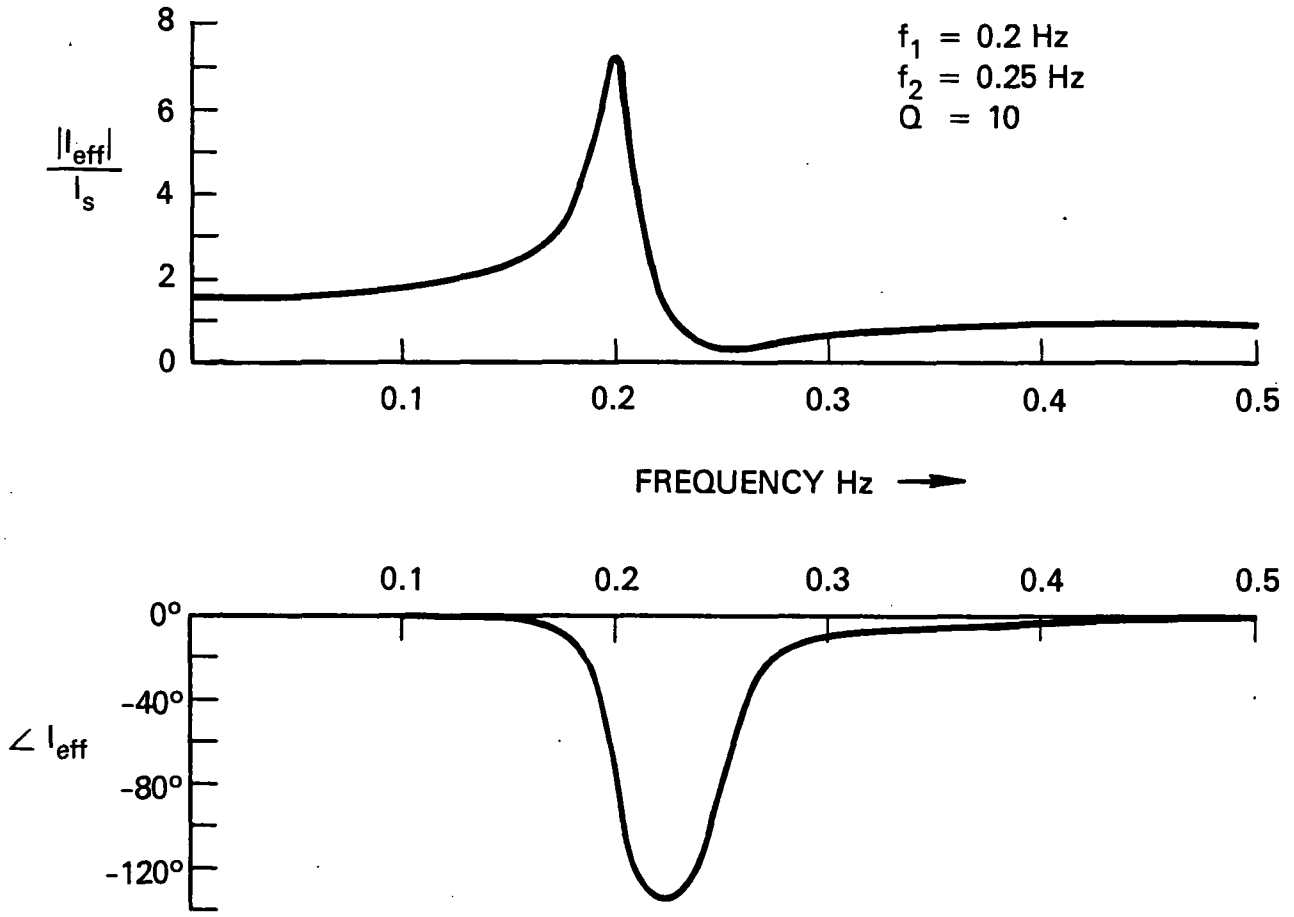

FIGURE 3.5. BOOM EFFECTIVE MOMENT OF INERTIA WITH FINITE Q (p. 1 of 2)

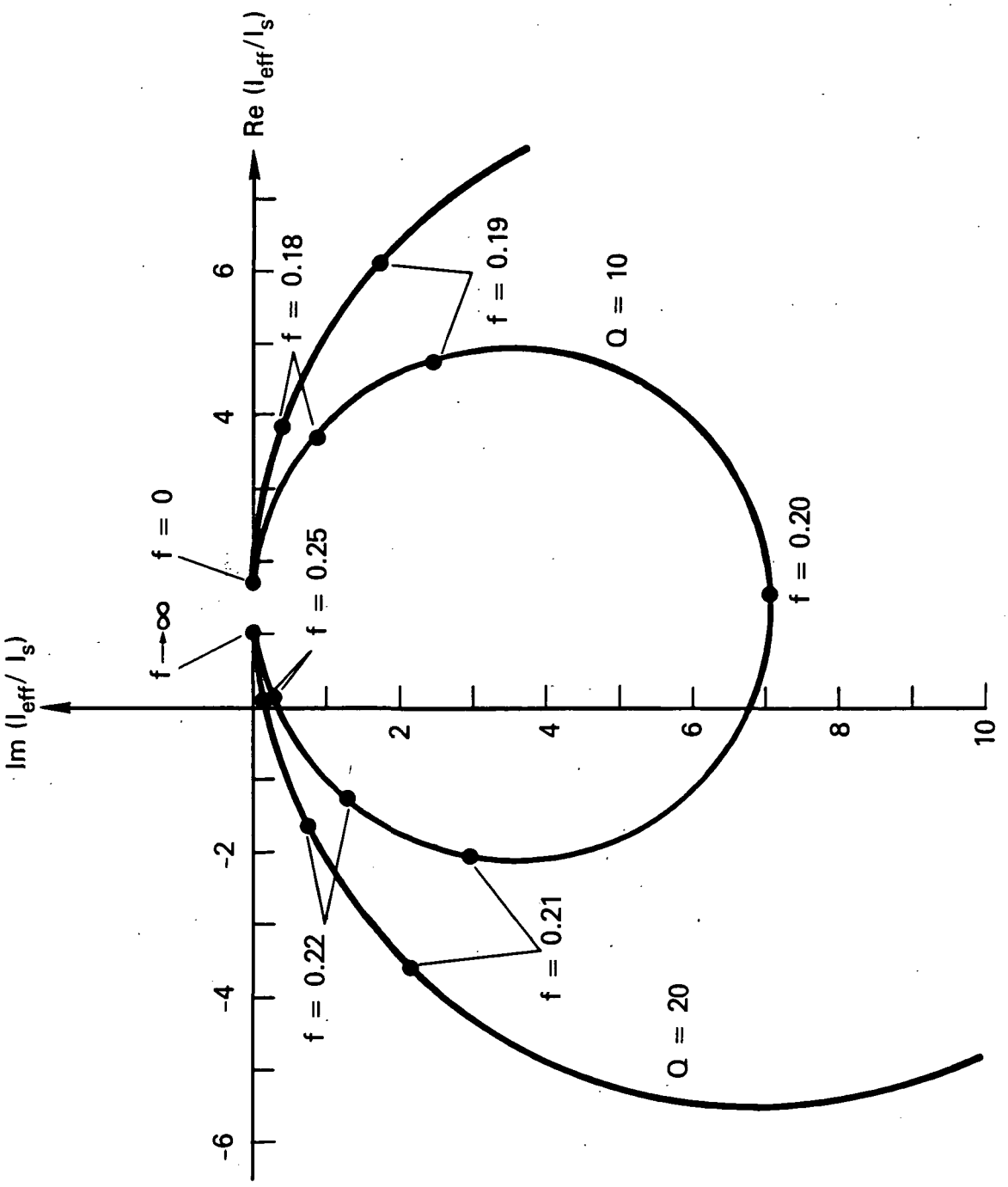

FIGURE 3.5. (p. 2 of 2)

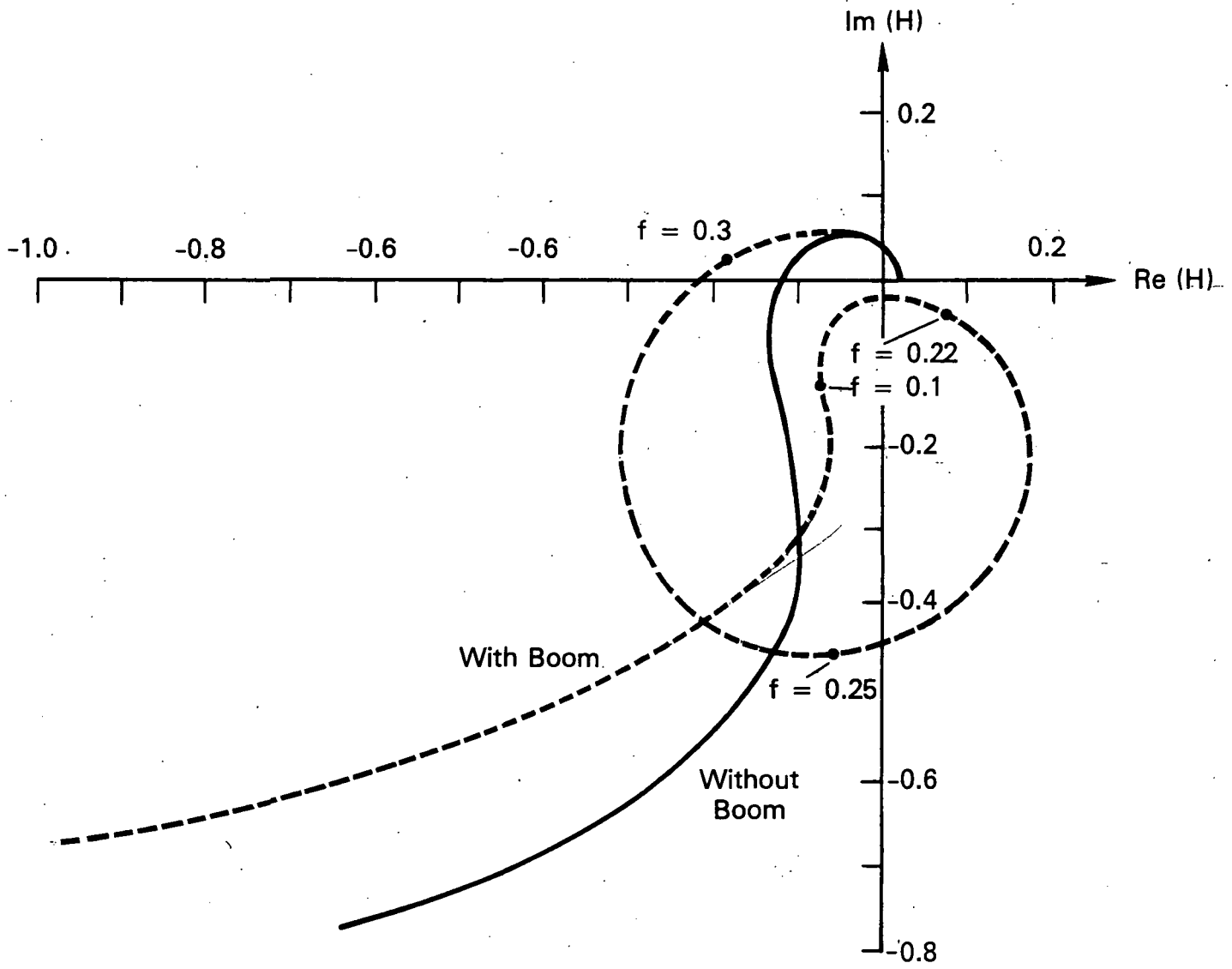

FIGURE 3.6. DETAIL OF NYQUIST CRITERION CONTOUR, WITH AND WITHOUT BOOM (DAMPING INCLUDED)

inserting a loop in the contour, and reducing the magnitude of the loop gain by a factor $I_s/(I_b + I_s)$ for all frequencies below about one-half f_1. From this it is seen that the stability of the system with the boom attached depends on two things:

- Whether the reduction in gain from the $I_s/(I_b + I_s)$ factor is sufficient to cause the contour to encircle the -1+j0 point.

- Whether the location and size of the loop in the contour are such that the -1+j0 point is encircled.

The reduction in gain must be at least a factor of 1/5 to cause instability, as observed earlier. This corresponds to a boom moment of inertia four times that of the spacecraft. (See Figure 2.12 for the implications of this.) The system would probably be rendered unstable for boom moments of inertia much smaller than this, however, because of the high values of Q. The value of Q used for the plot shown in Figure 3.6 was only ten. If Q were given a typical value of 300, the diameter of the loop in the H(s) contour would be much larger than that shown. The contour, with Q large, would almost surely encircle the -1+j0 point, unless the resonant frequencies were so placed that the loop in the contour fell mainly to the right of the origin. It is difficult to draw any general conclusions on the basis of this plot about what ranges of resonant frequency would or would not lead to instability. Fortunately, this is not necessary because it is possible to compensate the system to attenuate the effects of the resonance. This compensation is discussed next.

3.3 SYSTEM COMPENSATION

The speed of the response of a control system is tailored to the rate of variation of the outside disturbances acting on the system. For the TIROS-N attitude control system, these disturbances are the external torques described in Section 3.1. The system parameters were selected partly on the basis of how fast these torques varied. A number that is indicative of the system's speed of response is the frequency at which the loop gain is equal to one. Roughly speaking, we may say that the control system ignores all

spectral components of disturbance torque above this frequency. The frequency of unity loop gain for the TIROS-N system is 0.02 Hz.

The loop gain at low frequencies is reduced by the ratio of the spacecraft moment of inertia and the spacecraft plus boom moment of inertia, $I_s/(I_s+I_b)$, when a boom is attached. This has the effect of decreasing the frequency at which the loop gain is one. As a result, the response of the system is slowed down, as would be expected. This slowing must be compensated for, if the system is to perform as well as it did without the boom. The compensation consists of increasing the values of some parameters of the system in proportion to the increase in moment of inertia, so that the loop gain does not change. It is seen from the formula for loop gain (in Section 3.1) that there is a choice of parameters that could be increased to perform the compensation. For example, the gains, K_R, K_P, and K_I could all be increased by the same amount. But the simplest way to compensate for the increased moment of inertia is by increasing M, the reaction wheel motor constant. M is the ratio of motor torque to command voltage. The larger M, the more torque the motor produces for a given input voltage. A larger M generally means a larger, or at least more powerful, motor.

It is necessary to increase the maximum torque capability of the reaction wheel motor, as well as the motor constant, when compensating for the boom. This is required to maintain the same torque margin that existed without the boom present. This margin is necessary for the system to recover from intermittent malfunctions or computation errors, and is apparently quite large. The motors used in the TIROS-N are capable of producing a maximum torque of 10 oz.in (0.07 Nm), but according to telemetry records, they typically generate only about 2 percent of this on the average, and about 20 percent of this during short bursts.

Increasing the strength of the reaction wheel motor compensates for the effect of the boom for low frequencies, such that the speed of the control system's response is not changed. The other, high-frequency, effect of the boom must also be compensated for, so that stability of the system is maintained. This can be done by modifying the loop again in such a way that the poles and zeros represented by the boom resonance are cancelled out. The

modification consists, in effect, of inserting a filter in the system with a transfer function that matches exactly that of the effective moment of inertia.

Much of the signal processing in the attitude control system is performed digitally, using computer algorithms. It appears that the boom resonance filtering could be most easily incorporated into this digital processing. This would probably not require any hardware changes, although a faster processor may be needed if the additional computation time turned out to be excessive. Virtually any specified transfer function may be approximated by digital signal processing techniques, provided the frequency range over which it applies does not extend above half the sampling frequency. The sampling frequency is 2 Hz in the present case, so the digital filtering can only be performed in the 0-1 Hz frequency range. This is not a problem here because the first resonance almost always falls below one Hz.

The one Hz limitation means that the higher resonances lying above one Hz cannot be digitally filtered. It has been assumed in this study that higher mode resonances are at high enough frequencies that they are sufficiently attenuated by the natural rapid fall-off in loop response with frequency. This has not been specifically confirmed, however. If the higher mode resonances are found to be capable of inducing instability, it would be necessary to install analog filters in the system. These would be positioned before the samplers in Figure 3.1.

IV. ESTIMATION OF ANTENNA EXCURSIONS

The boom and control system analysis of the previous chapters will now be applied to estimate the magnitude of the interferometer antenna excursions due to boom dynamics. Estimates of the antenna movements due to thermal causes will also be determined. The combined effect of the boom behavior and other error sources on the accuracy of the interferometer system has been calculated using ORI's error simulation program. The results of these calculations are presented and discussed in Chapter 5.

4.1 ERROR SOURCES

An RF interferometer measures a signal's angle of arrival with respect to a baseline by comparing the signal RF phase as seen at the endpoints of the baseline. The angle of arrival is not explicitly determined in the process of calculating platform position from the phase difference. However, comparison of the angle of arrival errors from the various sources reveals the relative magnitudes and functional dependencies of the position estimation errors. Antenna displacements produce three types of errors in the apparent measured signal angle of arrival:

- Errors due to unknown deviation of the attitude of the actual baseline from that indicated by the spacecraft attitude sensor.

- Errors due to unknown changes in the length of the baseline. This changes the correspondence between measured RF phase angle and angle of signal arrival.

- Errors due to unknown changes in the relative orientations of the antennas. This introduces changes between actual electrical phase at the baseline endpoints and the signal phase measured at the antenna output.

The first type of error is purely geometric. Any unknown difference between the actual baseline attitude and the attitude sensed and telemetered by the spacecraft will directly contribute to the error in angle of arrival determination. Any such attitude error can be resolved into two components, only one of which contributes to angle of arrival error. Figure 4.1 shows the resolution of attitude error into components. The ellipses in the figure represent the circles described by the endpoints of the interferometer baseline when it is rotated about two axes. One rotation axis (I) is the line through the center of the baseline in the direction of signal arrival. The other axis (II) is through the center of the baseline in the direction normal to the plane formed by the baseline and the direction of signal arrival. An arbitrary attitude error can be resolved into rotations about these two axes, as shown. The error component about the I axis does not contribute to angle of arrival error, but the component about the II axis contributes directly. Throughout this study it has been assumed that dynamic antenna excursions were about the spacecraft's roll axis. This is the II axis for platforms located on the line normal to the subtrack.

The second type of error comes from the contraction or expansion of the baseline length due to thermal causes. The effect of this is seen from the formula relating electrical phase difference, ϕ, and angle of signal arrival, θ (see Figure 4.2):

$$\phi \text{ (radians)} = 2\pi(L/\lambda) \sin\theta$$

From this, we have

$$L = \lambda\phi/(2\pi \sin\theta)$$

$$dL/d\theta = -\lambda\phi(2\pi)^{-1}\sin^{-2}\theta \cos\theta = -L \cot\theta$$

$$\Delta\theta = -(\Delta L/L) \tan\theta$$

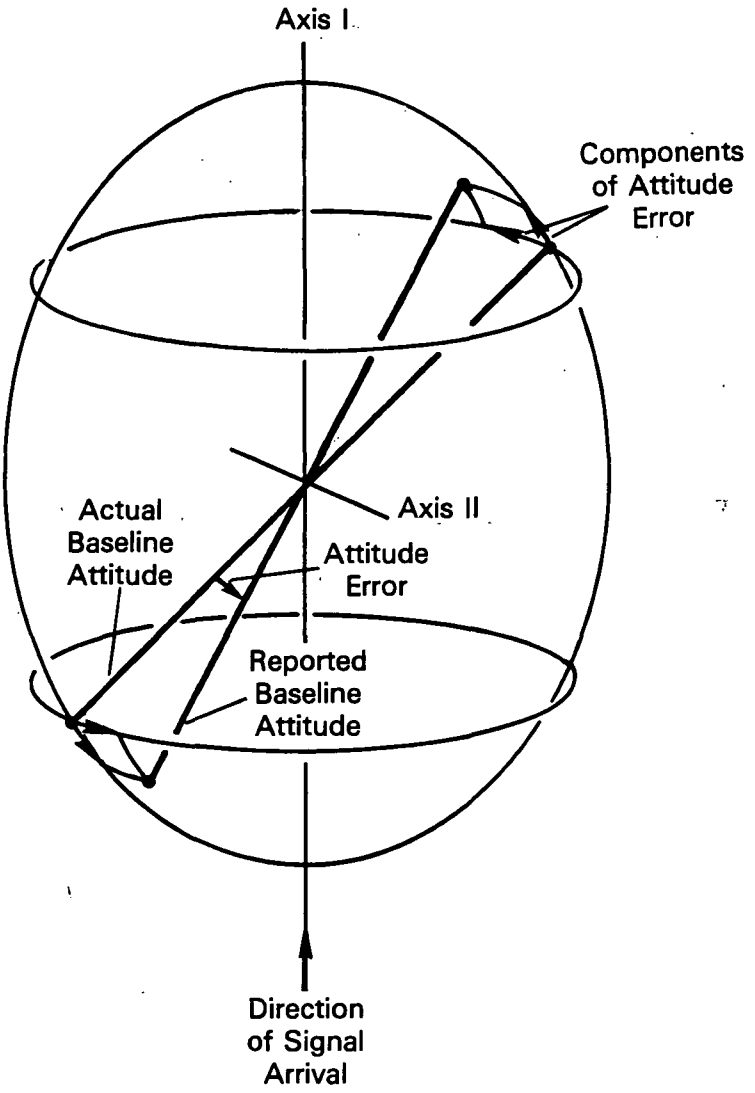

FIGURE 4.1. RESOLUTION OF ATTITUDE ERROR INTO COMPONENTS

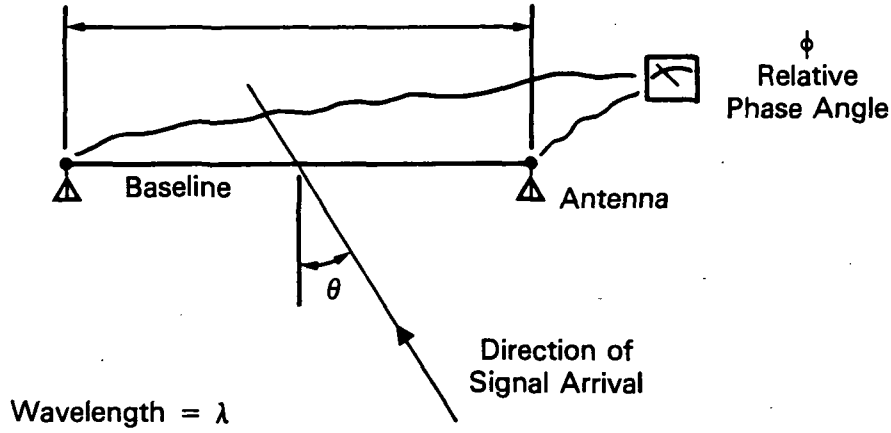

FIGURE 4.2. DEFINITION OF INTERFEROMETER PARAMETERS

This gives the angular error (in radians) corresponding to a small fractional change in the baseline length. The largest angle θ to be experienced in the case of the system envisioned is 58.7° (Corresponding to an 833 km satellite altitude and a 15° minimum elevation angle). For this worst case, then,

$$\Delta\theta(\text{degrees}) = 94.1\ (\Delta L/L)$$

A 1 percent change in baseline length, for example, would produce a maximum angle-of-arrival error of 0.94°.

The third type of error arises from the variation in phase response of the antennas as a function of angle of arrival. The antennas are assumed to be identical and mounted with their axes parallel. This means that a signal is received by each antenna from the same direction relative to its axes, and the phase delay is the same through both antennas. Relative phase errors can be introduced, however, when the antennas become misaligned by

flexing or twisting of the booms. The error in angle of arrival, $\Delta\theta$, produced by an antenna-induced phase error of $\Delta\phi$ is found from the basic interferometer equation:

$$\phi = 2\pi(L/\lambda)\sin\theta$$

$$d\phi/d\theta = 2\pi(L/\lambda)\cos\theta$$

$$\Delta\theta = \Delta\phi[2\pi(L/\lambda)\cos\theta]^{-1}$$

For the 58.7° maximum value of θ, this gives

$$\Delta\theta = 0.31\ (\lambda/L)\ \Delta\phi$$

A baseline of 40 m contains 53.3 wavelengths at 400 MHz, the anticipated operating frequency. For this case, the angular error produced by an electrical phase error of 1° is $(0.31)\ (53.3)^{-1}(1^\circ) = .006^\circ$.

The question of how much phase error can result from a given antenna misalignment is difficult to determine. Indications are, however, that the variations in phase response are not appreciable over the ± 60° field-of-view of the antenna type contemplated. The most variation expected is one electrical degree per physical degree of antenna misalignment. Thus errors from this source appear negligible.

4.2 ESTIMATION OF ANTENNA DISPLACEMENTS

In the following analyses, the displacements of the antennas at the endpoint(s) of the interferometer boom(s) are estimated, based on these simplifying assumptions:

- The interferometer baseline is aligned with the spacecraft's pitch axis (normal to the orbit plane) and only displacements along this axis and about the roll and yaw axes produce any significant errors.

- Dynamic and thermal displacements about the yaw axis are approximately the same as those about the roll axis. (Only the latter will be calculated.)

- The interferometer is aboard the TIROS-N spacecraft, in a 833 km sun-synchronous orbit.

- The spacecraft attitude control system has been compensated by increasing the reaction wheel motor constant in proportion to the increase in spacecraft moment of inertia due to the boom(s), and incorporating filtering as discussed in Chapter 3.

- The interferometer uses either one or two booms.

- Unknown antenna displacements are random with zero mean value, and those from different sources are independent.

4.2.1 Dynamic Displacements

The transfer function, T(f), relating boom end-point displacements to the moment applied at the spacecraft center of mass (assuming sinusoidal time variation) was determined in Chapter 2. The variance of the random end-point displacement, σ_y^2, is given by [8]

$$\sigma_y^2 = \int_0^\infty S_m(f) \left| T(f) \right|^2 df$$

Where $S_m(f)$ is the power spectral density of the random component of the applied moment. The random component of the moment excludes the constant (secular) component and the component that varies cyclically over the orbit period. $S_m(f)$, and T(f) with damping considered, are estimated next.

4.2.1.1 Estimation of $S_m(f)$. The power spectral density of the random applied moment could be estimated by performing a spectral analysis of the momentum wheel motor command voltage, which is telemetered to the ground. A one-orbit record of the command voltage [5] is shown in Figure 4.3. This was not done, however. Rather, an analytical procedure was used that is sufficiently accurate for present purposes. $S_m(f)$ was determined to within

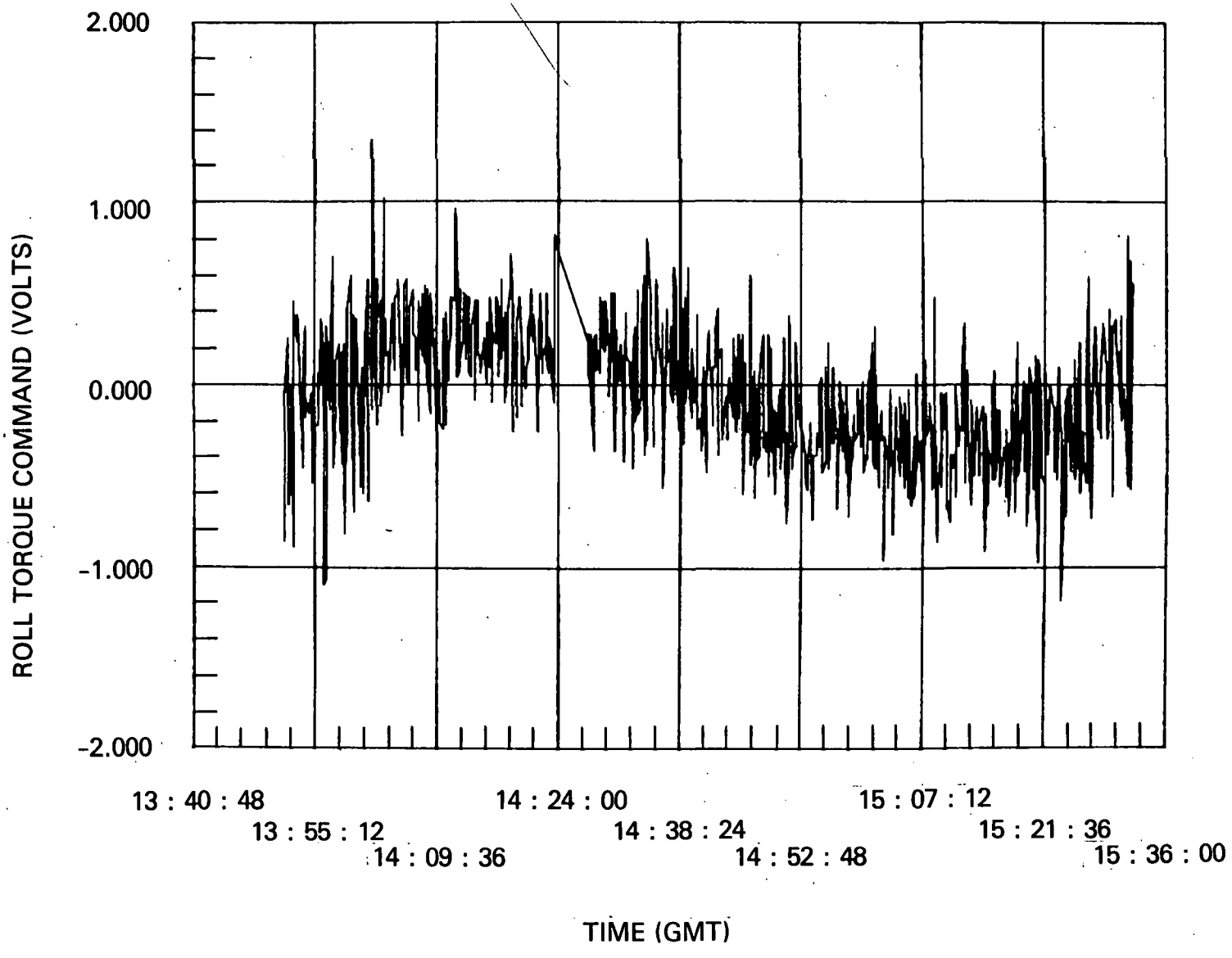

FIGURE 4.3. TELEMETRY RECORD OF TORQUE COMMAND FOR TIROS-N

a constant multiplier by assuming that the random torque originated from a noisy reference in the earth sensor, and that the noise of the reference was white, or had a constant power spectral density. The frequency dependence of power spectral density of the motor command voltage was then determined from the attitude control system transfer function. The value of the constant multiplier was set to that which gave a control voltage variance equalling the value estimated from the record in Figure 4.3. The details of this procedure follow.

The transfer function relating the motor command voltage, C, to the attitude sensor reference θ_r, may be determined from Figure 3.1. By setting $\dot{\theta}_r = 0$ and writing the equations from the diagram, we obtain

$$A(f) = C/\theta_r = \frac{E(f)(k_p - jK_I/2\pi f)}{1 + H(f)} \cdot \frac{\sin \pi f}{\pi f}$$

where H(s) is the loop gain calculated earlier, as compensated to eliminate boom effects. The $\sin(\pi f)/\pi f$ term of A(f) comes from the 0.5-second sampling at the earth sensor and structural filter outputs.

The earth sensor reference noise is assumed to have a constant (single-sided) power spectral density

$$S_{\theta_r}(f) = N_0 \text{ rad}^2/\text{Hz}$$

The power spectral density of the motor command voltage is then given by

$$S_C(f) = |A(f)|^2 S_{\theta_r}(f) = N_0 |A(f)|^2 \text{ v}^2/\text{Hz}$$

This can be integrated to obtain the command voltage variance:

$$\sigma_C^2 = \int_0^\infty S_C(f)\, df = N_0 \int_0^\infty |A(f)|^2 df \quad \text{v}^2$$

The integral has been evaluated numerically from the plot of A(f) and is equal to 1.15×10^6 v^2/rad^2. The command voltage standard deviation σ_C has been estimated from the telemetry record of Figure 4.3 to be 0.25 v. Thus $N_0 = 5.4 \times 10^{-8}$ rad^2/Hz. $S_C(f)$, using this value for N_0 is shown in Figure 4.4.

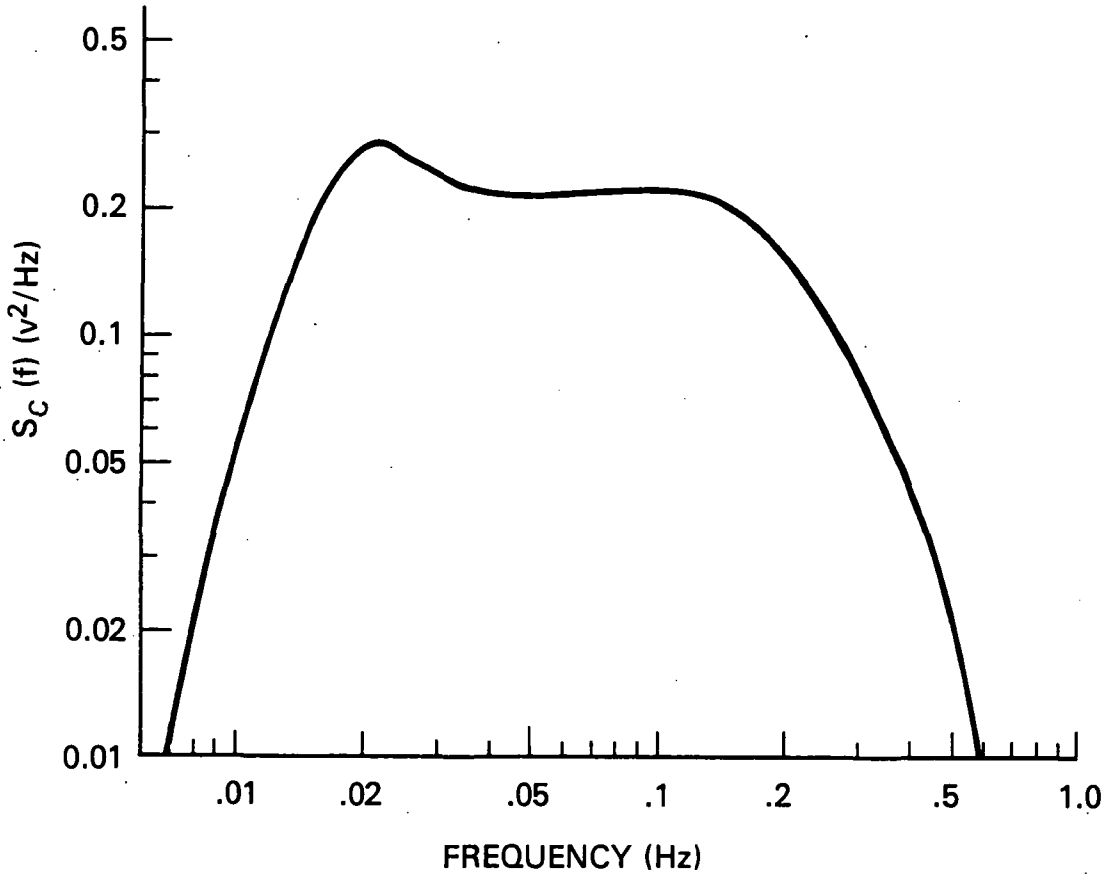

FIGURE 4.4. ESTIMATED COMMAND VOLTAGE POWER SPECTRAL DENSITY

The power spectral density of the random moments applied to the spacecraft by the reaction wheel motor is given by

$$S_m(f) = M^2 S_C(f)$$

The motor constant M will be varied in proportion to the total spacecraft plus boom moment of inertia to obtain values of $S_m(f)$ for varying boom lengths. Note that M also appears in H(f), the loop gain, which went into determining $S_C(f)$. This will cause no difficulty, however, because M appears in H(f) only in the ratio M/I. M is varied in proportion to I, the total moment of inertia, so the ratio is unchanged and H(f) is unchanged while varying M.

4.2.1.2 Estimation of T(f) With Damping. The transfer function relating the boom endpoint (antenna) displacements to the applied moment, T(f), has been found for the case of zero damping. T(f) will be estimated with damping by considering the analogous dynamic system discussed in Section 2.7. The transfer function for the analogous system will be found as a function of its Q, and this functional relation will be applied to the boom transfer function.

The solution to the analogous system can be put into the form of a transfer function as follows. (Refer to Figure 2.13 for definition of symbols.)

$$T = (y_2 - y_1)/M_o = (L/I)[\omega^2 - j\omega\gamma u - ku]^{-1}$$

where

$$u = (mI)^{-1}(I + mL^2)$$

If we define

$$\omega_2 = \sqrt{ku} = \text{undamped resonant frequency}$$

$$Q = k/(\gamma\omega_2)$$

The magnitude of the transfer function becomes

$$T(\omega) = \left|T(0)\right| \left| \omega_2^2 \left[\omega^2 - j\omega(Q/\omega_2) - \omega_2^2\right]^{-1} \right|$$

where $\left|T(0)\right|$ is the transfer function magnitude at zero frequency:

$$\left|T(0)\right| = Lm \left(I + mL^2\right)^{-1} k^{-1}$$

The Q defined above has the same relation to the damping time constant, resonant frequency, and the logarithmic decrement for this model, as does the Q defined earlier for the boom.

An essential feature of the analogous system is that its transfer function, when Q is infinite (no damping), behaves in the same way as the boom transfer function, in the frequency range of zero to the first resonance. We will not be concerned with boom resonances beyond the first, so the spring-mass system can serve as an approximation to the boom system. In particular, it can be used to approximate the behavior of the boom with damping. With a finite, but large, value of Q, the maximum value of the spring-mass transfer function occurs very near ω_2, and its value is very nearly given by

$$\left|T(\omega)\right|_{max} \simeq Q \left|T(0)\right|$$

Applying this to the spacecraft/boom system, we see that the effect of damping on the boom transfer function is to put a limit on the peak value at the first resonance equal to Q times the value at zero frequency. It also widens the peak so that its width at $0.707 \left|T(\omega)\right|_{max}$ is the resonant frequency divided by Q.

4.2.1.3 Estimation of Dynamic Excursion Variance. The variance of the dynamic displacement can now be calculated from the formula

$$\sigma_y^2 = \int_0^\infty S_m(f) \left|T(f)\right|^2 df$$

using the estimates of $S_m(f)$ and $T(f)$. The calculation is considerably simplified by the high values of Q for the boom. When Q is large, the only significant contribution to the integral is in the frequency range very near the resonant frequency. In this narrow range, the value of $S_m(f)$ can be approximated by its value at the resonant frequency, or $S_m(f_o)$. With this approximation, and recalling that $S_m = M^2 S_C$, we have

$$\sigma_y^2 \simeq M^2 \, S_C(f_2) \int_0^\infty |T(f)|^2 d\, f$$

the integral is evaluated with the help of a table [9] to obtain

$$\sigma_y^2 \simeq M^2 \, S_C(f_2) \, T^2(0)(\pi/2) f_2 \, Q$$

The motor constant M for the TIROS-N attitude control system is 0.122 in-lb/v, or 0.0138 N-m/v. When the boom is added, the attitude control system is assumed to be augmented by multiplying the motor constant by the ratio $(I_b + I_s)/I_s$, where I_s and I_b are the moments of inertia of the spacecraft and boom, respectively. I_s and I_b are given in Figure 2.12. The zero frequency transfer function value, T(0), which is the displacement with a constant 1 N-m applied torque, is given in the same figure. The first resonant frequency of the boom as a function of length is given in Figure 2.11. As discussed in Chapter 2, Q is taken to be a linear function of the boom length to diameter ratio L/D:

$$Q \simeq 5 \, L/D$$

Up to now, a single-boom interferometer (the alternate configuration in Figure 1.1) has been assumed. However, a two-boom configuration offers better dynamic performance and would have less of an impact on the attitude control system, so it should be considered as well. The moment of inertia added by the booms when two booms are used is twice the moment of inertia of one boom of half the baseline length. This is substantially less than that of one boom of the whole baseline length. The resonant frequency is also higher for two booms compared with one boom with the same baseline length.

The standard deviation of the boom endpoint displacement, σ_y, has been calculated as indicated above for the single-boom and two-boom configurations, and it is shown in Figure 4.5 as a function of baseline length. The boom types used were the ten-inch and twenty-inch diameter Astromast. σ_y appears to increase approximately as the fifth power of boom length. The values of σ_y given for the two-boom case apply to the end point of one of the booms. When determining interferometer location and velocity estimation errors for this case, it must be assumed that the endpoints of the two booms are always displaced in opposite directions. The standard deviation of the angle of arrival error corresponding to σ_y is then twice the boom length times σ_y.

4.2.2 Thermal Displacements

Three types of thermally-produced antenna displacements are to be expected: Linear displacements along the boom axis due to boom contraction and expansion, linear displacements perpendicular to the boom axis due to flexing of the boom, and angular displacements due to twisting of the boom. The first of these is given by the coefficient of thermal expansion of the boom material and the temperature difference expected. The other two can be estimated based on information provided by Astro Research Corporation.

When the spacecraft passes from the day to the night part of its orbit, the temperature of the boom changes from about 200°F to -50°F. The coefficient of thermal expansion of the boom longeron material (fiberglass) is 2.8×10^{-6}/deg F. The total length change ΔL is therefore given by

$$\Delta L \simeq 7 \times 10^{-4} L$$

This length change is predictable, since the times when the spacecraft passes between day and night are known. There will be errors in the prediction, however, mainly from two sources: (1) Varying earth albedo partly determines the temperatures of the boom, and it is not possible to predict this. (2) There is a large thermal transient as the spacecraft passes between sun and

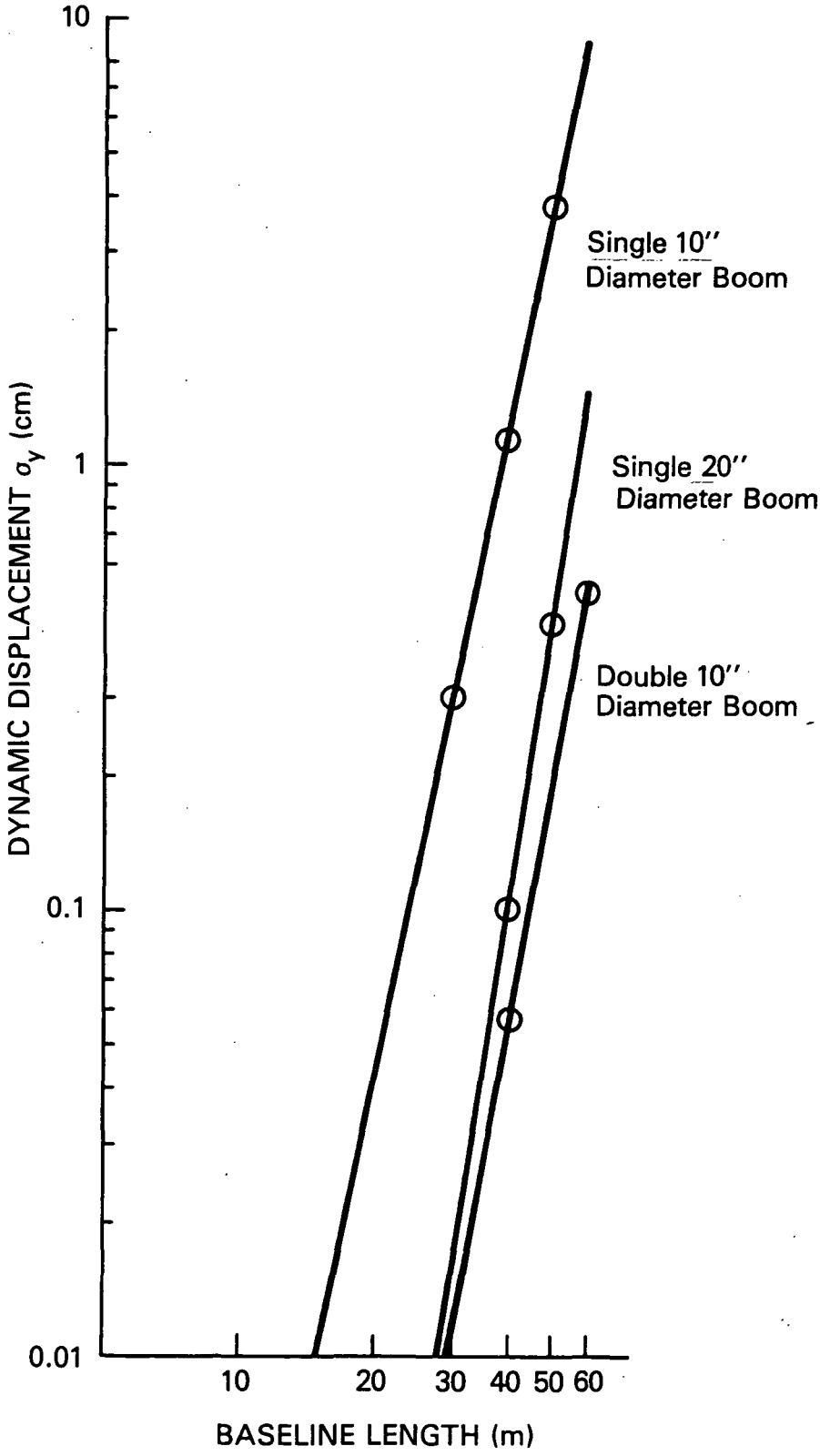

FIGURE 4.5. ANTENNA DYNAMIC DISPLACEMENT STANDARD DEVIATION

shadow, and there will be an error in predicting the time-variation of the length during the transient. Considering these prediction errors, the standard deviation of the unknown component of length change, averaged over an orbit, is judged to be about 20 percent of the total change, or

$$\sigma_{\Delta L} \simeq 1.4 \times 10^{-4} L$$

The endpoint displacement due to thermal bending of the boom can be estimated using the following formula [3]

$$\Delta y = (1/2)\, \alpha(\Delta T) d L^2/(8r^2)$$

where

Δy = Endpoint displacement
α = Coefficient of thermal expansion
ΔT = Temperature difference across boom
d = Diameter of longeron
r = Radius of boom
L = Length of boom

Using α for fiberglass, given earlier, the empirical relation for continuous longeron Astromasts $d/D = 0.015$, and $\Delta T = 5.5^\circ$ F [3], this becomes

$$\Delta y = 5.8 \times 10^{-8} L^2/D$$

For the ten-inch diameter Astromast, this comes to only about 0.6 mm for a 50 m boom, so it can be neglected in comparison with other displacements.

Twisting of the boom due to thermal radiation arises from the varying sun angle on the diagonal wires of the boom. The twisting is prevented to large degree by constructing the boom with a pre-twist, so that a small twist (usually one turn over the length) remains in the boom after it is deployed. Data supplied by Astro Research Corporation shows that the worst case thermal twist for an Astromast boom is given approximately as a function of the length to diameter ratio L/D by

$$\text{twist (deg)} = 8.5 \times 10^{-7} \, (L/D)^{2.5}$$

For a 50 m long ten-inch diameter Astromast, the twist is about 0.45°. If the antenna phase response changes by one electrical degree per physical degree, this would introduce a 0.45° phase error for a single-boom system, which may be substantial. Note that for a two-boom system the net thermal twist between antennas could be made near zero by constructing the booms so that they twist in the same direction with respect to the spacecraft. It may be possible to predict the thermal twist on the basis of the sun angle, but due to the geometric complexity of the boom and the effect of earth albedo, such prediction would probably have a fairly large error. The standard deviation of the error in predicting the thermal twist would probably be on the order of half of the twist magnitude, or

$$\sigma_{twist} \approx 4 \times 10^{-7} \, (L/D)^{2.5}$$

V. LOCATION/VELOCITY ESTIMATION

Previous studies [1] have indicated that the combination of differential doppler and interferometer measurements on board a low-altitude satellite enables estimation of platform position and velocity with errors strongly dependent upon the length of the interferometer baseline(s). However, these studies did not incorporate the degrading effects of interferometer boom flexure which, as shown in Chapter 4, can become significant.

5.1 BOOM FLEXURE

The analyses of Chapter 5 derived the standard deviation of the displacement of a boom tip relative to a rigid boom while being controlled in attitude by a system typified by that on board TIROS-N. Because these displacements occur as a result of noise in the attitude control system, these flexural displacements will occur in random directions and essentially in a plane perpendicular to the non-deformed boom axis. However, because the interferometer measures the angle of the platform relative to the interferometer axis, only those flexural displacements occurring in the plane containing the interferometer axis and the platform will affect performance. The effect of these displacements is to increase the effective attitude error associated with the orientation of the interferometer axis, as can be seen in the sketch shown in Figure 5.1 for the case of two booms forming the baseline.

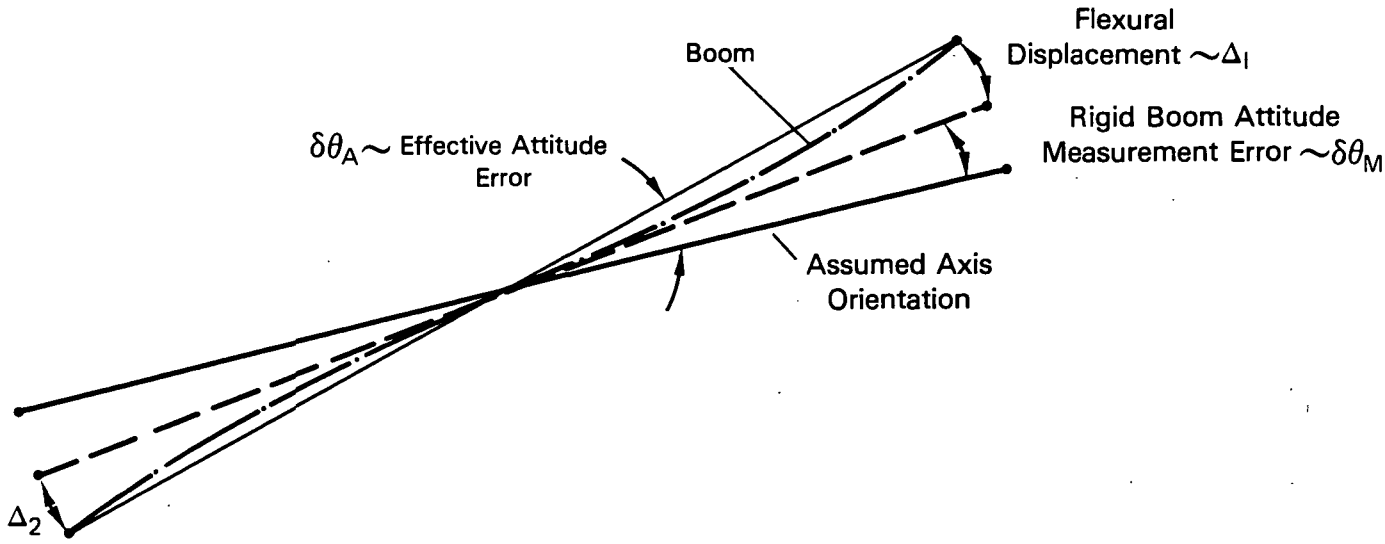

FIGURE 5.1. ATTITUDE ERROR

From this sketch, the effective attitude error can be derived as

$$\delta\theta_A = \delta\theta_M + (\Delta_1 - \Delta_2)/2L$$

where L is the baseline length.

In order to evaluate location/velocity errors as a result of this effective attitude error, the standard deviation of the effective attitude error is required. For present purposes, two conservative assumptions are made:

- The flexural displacements derived in Chapter 4 are assumed to occur in the plane formed by the interferometer axis and the platform.

- For the two-boom baseline, the flexural displacements of the two tips are assumed to be out of phase - i.e., the displacements always add to result in the largest effective attitude error.

With these assumptions, the standard deviation of the effective attitude error for a two boom baseline is

$$\sigma_{\theta_A} = \sqrt{\sigma^2_{\theta_M} + 2(\sigma_\Delta/L)^2}$$

while for the single boom baseline

$$\sigma_{\theta_A} = \sqrt{\sigma^2_{\theta_M} + (\sigma_\Delta/L)^2}$$

5.2 LOCATION/VELOCITY ERRORS

To evaluate the performance of the doppler-interferometer system, two configurations of interferometers have been analyzed as a function of baseline length. One of these is a single axis interferometer oriented parallel to the earth's surface and perpendicular to the orbital plane. The other configuration is a cross-arm interferometer whose plane is parallel to the earth's surface and whose axes are 45^o to the orbital plane. Both configurations should take most advantage of the complimentary characteristics of doppler and interferometer measurements.

The performance of the doppler/interferometer configurations is shown in Figures 5.2 through 5.6 in terms of the standard deviation of the maximum velocity error component* (east or north) versus the baseline length. As noted, several conditions are different for each figure while other conditions are the same for all data. The common conditions are:

- 10^o longitude separation. (This is the separation between the platform and sub-track of the satellite at point of closest approach with the platform located at the equator.)

*For all configurations, location errors are all less than one kilometer when velocity errors approach one to two meters/second.

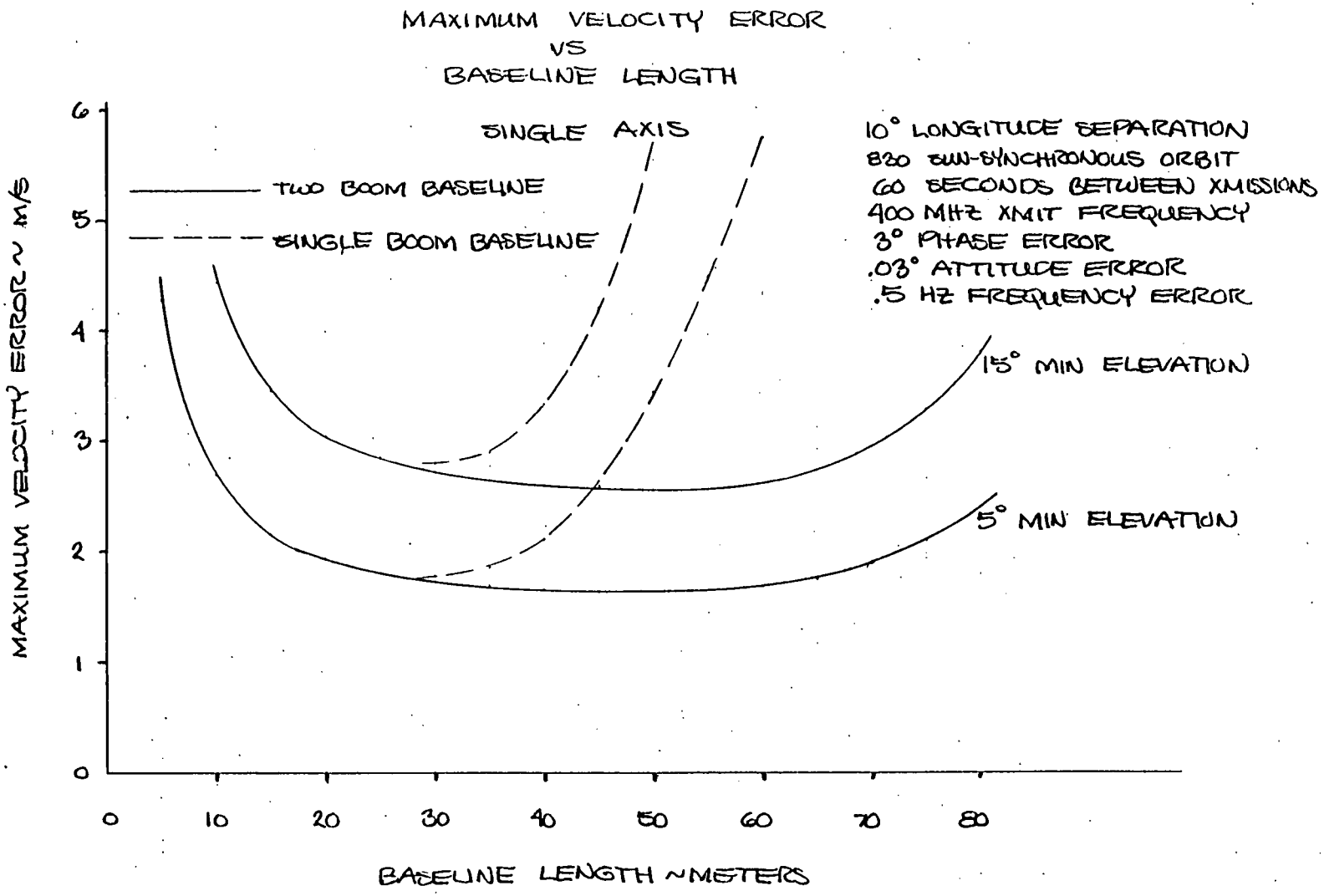

FIGURE 5.2. VELOCITY ERROR FOR SINGLE AXIS AND READILY ACHIEVABLE MEASUREMENT ERRORS

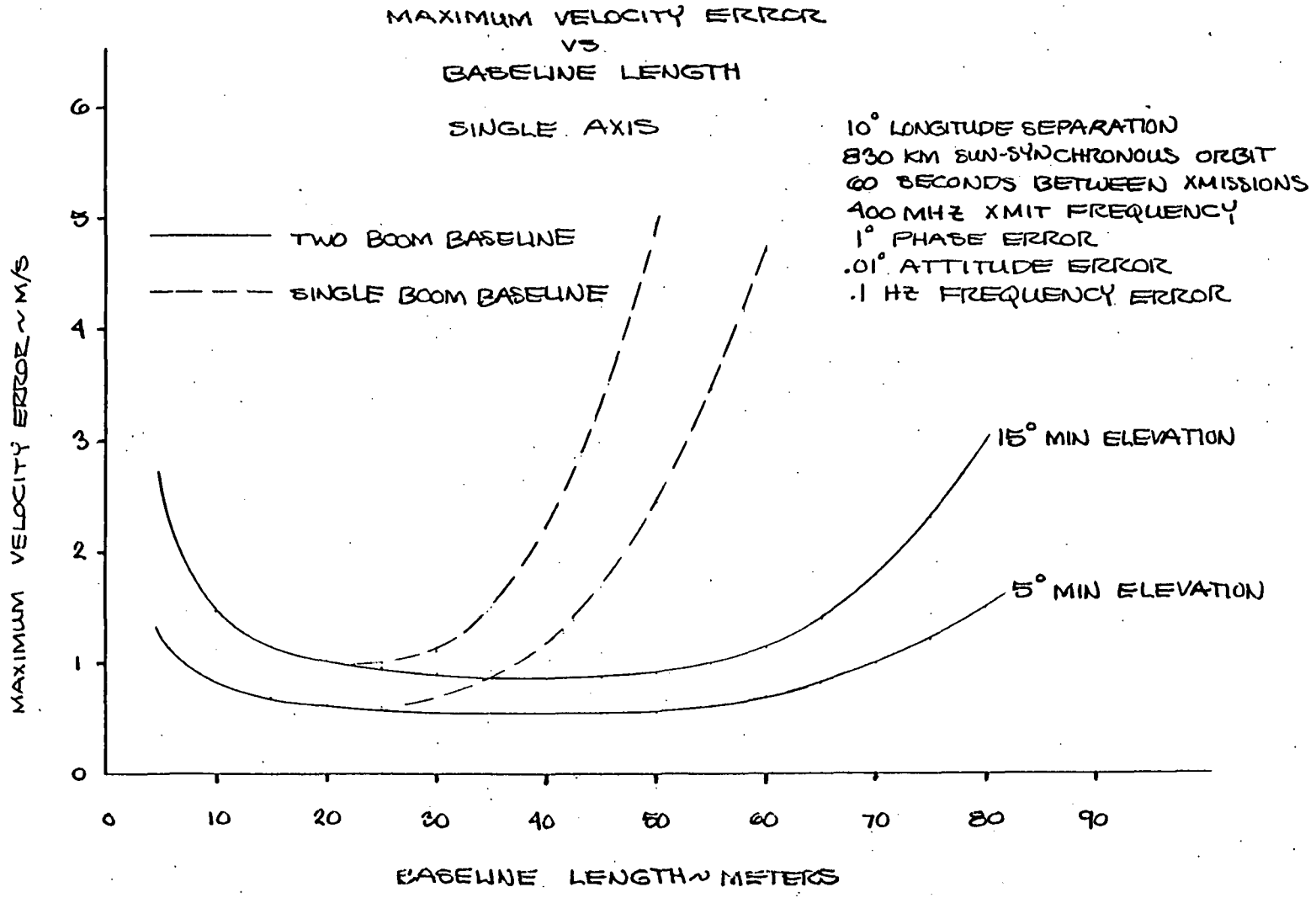

FIGURE 5.3. VELOCITY ERROR FOR SINGLE AXIS AND OPTIMISTIC MEASUREMENT ERRORS

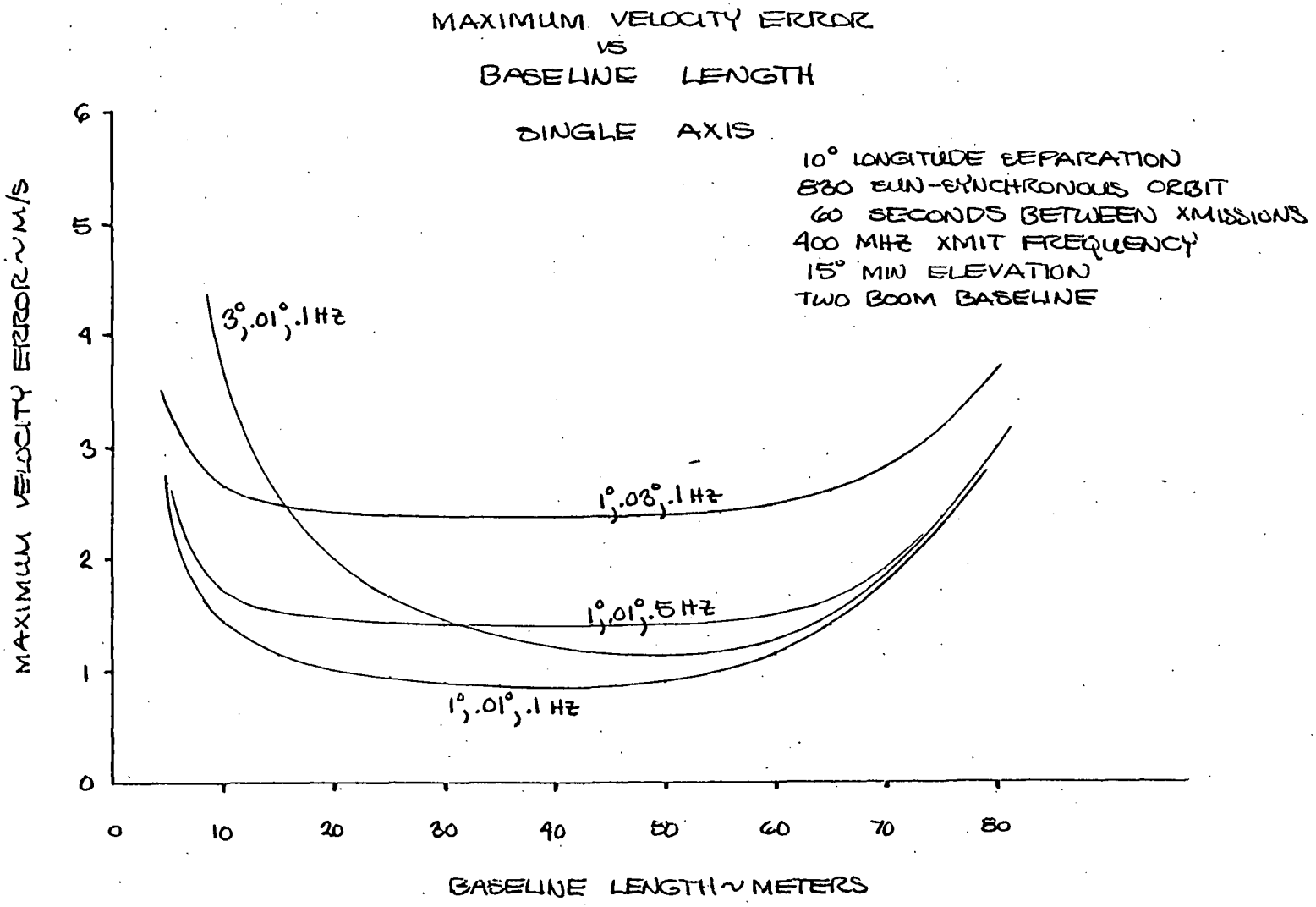

FIGURE 5.4. VELOCITY ERROR FOR SINGLE AXIS AND COMBINATIONS OF MEASUREMENT ERRORS

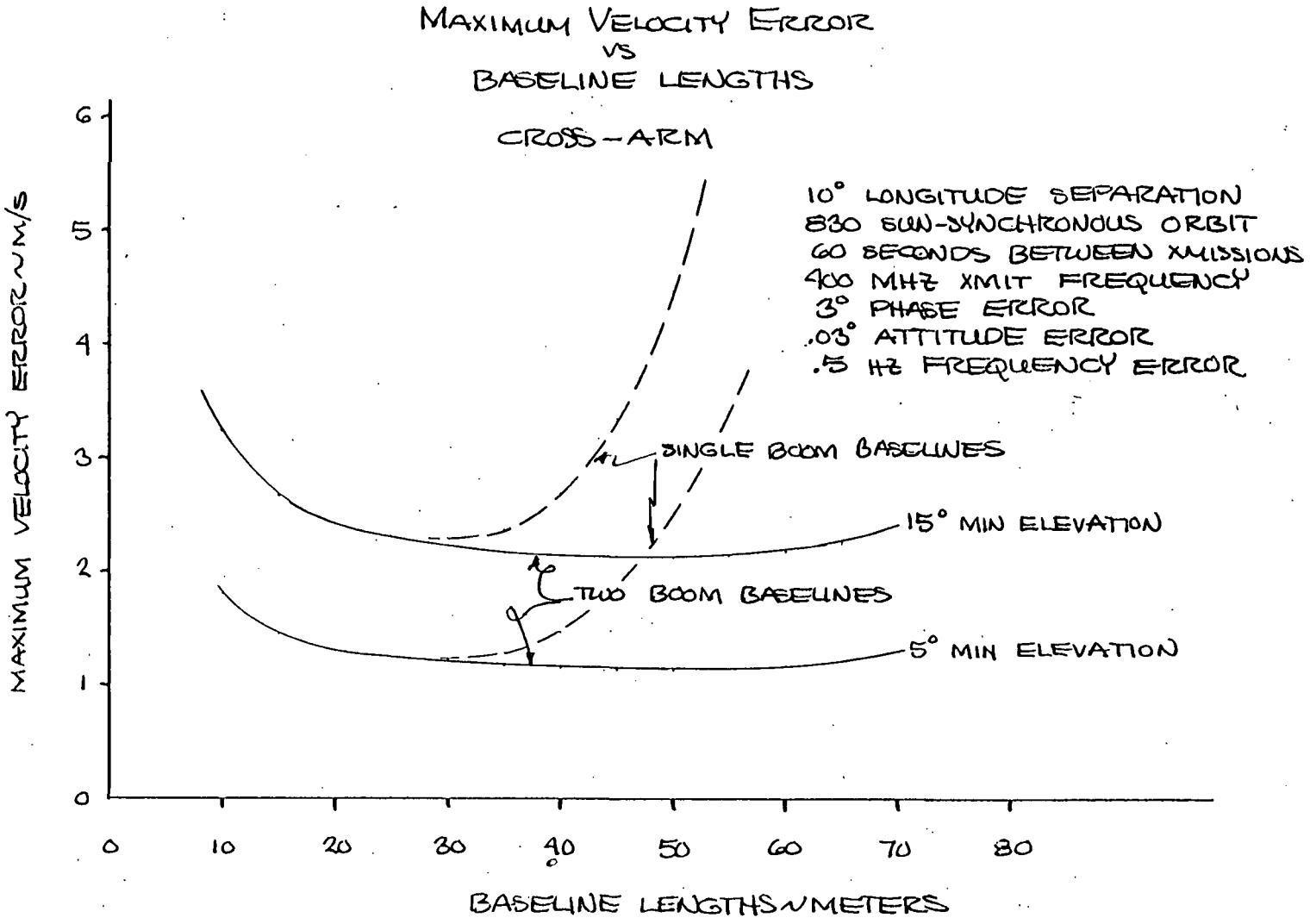

FIGURE 5.5. VELOCITY ERROR FOR TWO AXES AND READILY ACHIEVABLE MEASUREMENT ERRORS

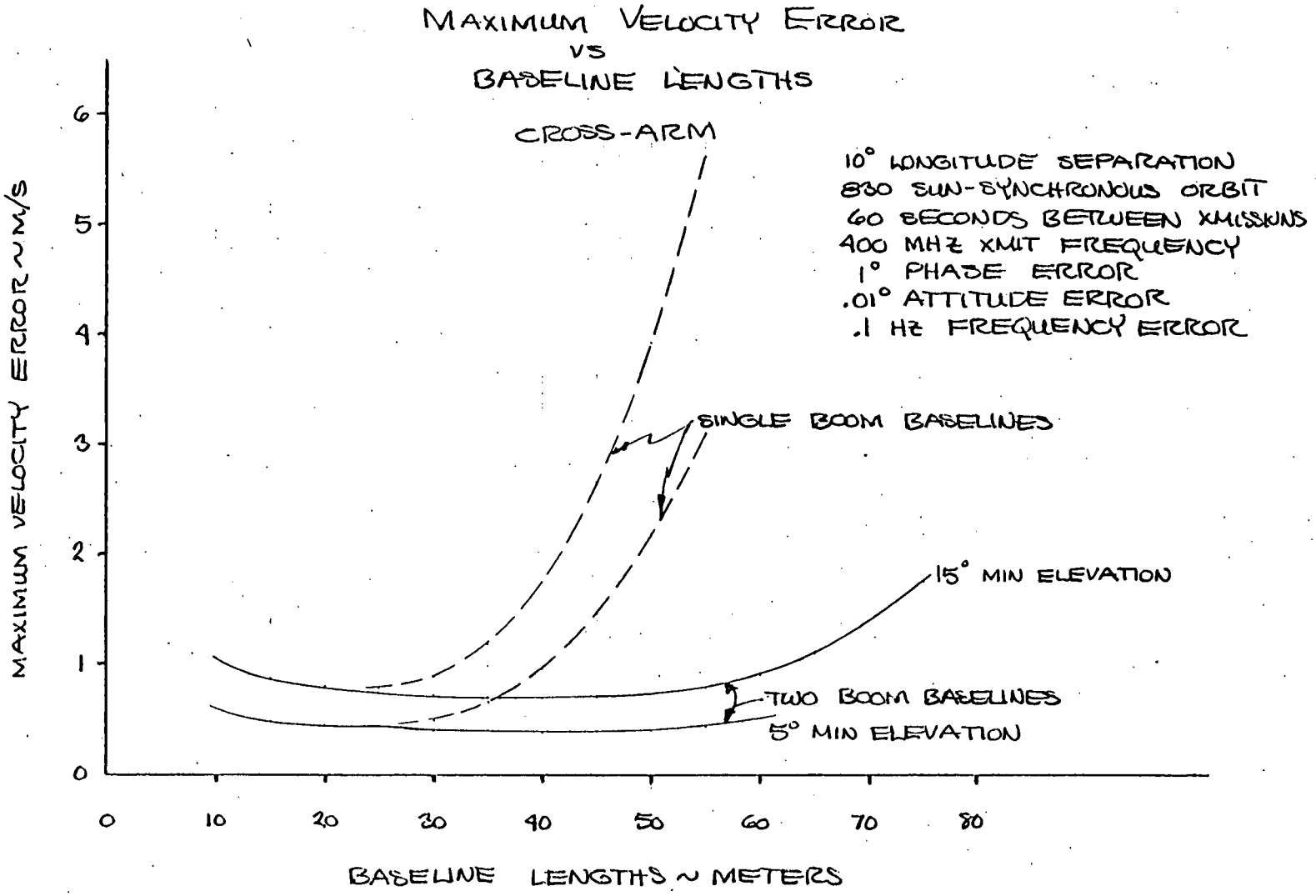

FIGURE 5.6. VELOCITY ERROR FOR TWO AXES AND OPTIMISTIC MEASUREMENT ERRORS

- 830 kilometer sun-synchronous orbit
- 60 seconds between transmissions from the platform to the satellite
- 400 MHz transmit frequency of the platform.

The conditions which are parametrically varied from one figure to another pertain to:

- The minimum elevation of the satellite above local horizontal at the platform that permits reception of useful transmissions at the satellite. For the data two minimum elevation angles of 5^{o} and 15^{o} are used. For the geometry established by the 830 Kilometer orbit, the 10^{o} longitude separation, and the 60 seconds between platform transmissions, the 5^{o} elevation angle results in the reception of eleven transmissions at the satellite while the 15^{o} elevation angle results in seven transmission receptions at the satellite.

- Whether the interferometer baseline(s) are achieved with one cantilevered boom from the satellite, or with two equal length booms

- The standard deviation of the error in measuring the relative phase between interferometer receivers

- The standard deviation of the spacecraft attitude measurement error. (Presumed to be identical to the attitude error associated with describing the orientation of the line between the phase centers of differencing receiver pairs.)

- The standard deviation of the error in measuring received frequency.

In Figures 5.2 and 5.3, the performance of the single, horizontal axis interferometer is shown, with Figure 5.2 corresponding to standard deviations of phase, attitude, and frequency measurement errors of 3^{o}, $.03^{o}$, and .5 Hz respectively, while Figure 5.3 corresponds to errors of 1^{o}, $.01^{o}$, and .1 Hz. In this regard, Figure 5.2 is considered to be representative of performance with readily achievable measurement errors while Figure 5.3 is considered to be representative of performance with optimistic measurement errors. Perusal of these figures leads to the following conclusions:

- Baseline lengths greater than 25 to 30 meters do not appreciably improve performance and there is no distinct advantage of the double boom baseline over the single-boom baseline for these lengths.

- Velocity errors are nearly halved by a system capable of operating down to minimum elevation angles of 5^{o} compared to 15^{o} - this is due to increased noise filtering (eleven versus seven transmissions received) as well as the longer time span over which measurements are taken.

- In order to meet a one meter/second estimation error, the measurement errors required need to be less than those assumed for Figure 5.2 but greater than those of Figure 5.3 when the baseline length can be near 25 to 30 meters.

In Figure 5.4, the effects of the three measurement errors of phase, attitude, and frequency are indicated. As noted, the lowest curve corresponds to velocity errors for the lower values of the measurement errors used for Figure 5.3 and in fact the lower curve of Figure 5.4 is identical to the 15^{o} minimum elevation curve of Figure 5.3. The other curves of Figure 5.4 indicate the change in performance if all parameters of Figure 5.3 are held

fixed with the exception of one of the measurement errors. This one exceptional measurement error is assumed to take on the value used in Figure 5.2.

At the nominal baseline lengths of 25 to 30 meters, the data of Figure 5.4 indicate that the degradation in performance is about the same for the 0.1 Hz to 0.5 Hz increase in frequency measurement error as it is for the 1^{o} to 3^{o} increase in phase measurement error. However, the 0.01^{o} to 0.03^{o} increase in attitude error significantly degrades performance. Also, for baseline lengths less than 15 to 20 meters, the phase measurement error clearly becomes the dominant error source.

In Figures 5.5 and 5.6, the performance of the cross-arm interferometers are shown, with Figure 5.5 representing performance at the higher values of measurement errors. Comparison of these data with the single axis performance data of Figures 5.2 and 5.3 shows the following:

- There is little justification for baseline lengths longer than 25 meters and little difference between single and two boom performance at this length or lower.

- The improvement in performance is on the order of 40 percent to 50 percent for the cross-arm compared to single axis interferometer and nearly permits achieving one meter/second velocity errors at the larger values of measurement errors.

REFERENCES

1. Reed, D. L. and R. G. Wallace, "NOSS/ALDCS Analysis and System Definition - Final Report," ORI Technical Report 1864, prepared for NASA/GSFC under contract NAS5-26164, Mod 1, February, 1981.

2. Teleki, C., "State-of-Art Survey of Extendible Structures for a Spacecraft-Mounted Long Baseline Interferometer," ORI, Inc., October 1977.

3. "Astromasts for Space Applications," paper ARC-B-004, Astro Research Corporation, Santa Barbara, California, August 1978.

4. Morse, P. M., Vibration and Sound, McGraw Hill Book Co., New York, 1936.

5. Andary, J., and C. Dunker, "TIROS-N Attitude Determination and Control System," NASA Doc. No. X-480-79-14, Goddard Space Flight Center, April 1979.

6. TIROS-N ADACS design information provided by J. Andary, GSFC.

7. Kuo, B. C., Automatic Control Systems, Prentice-Hall, Inc., Englewood Cliffs, N. J., 1962.

8. Papoulis, A., Probability, Random Variables, and Stochastic Processes, McGraw-Hill Book Company, New York, 1965.

9. Gradshteyn, I. S. and I. M. Ryzhik, Table of Integrals, Series, and Products, Academic Press, New York, 1965, Integral No. 3.242.

APPENDIX A
INTERFEROMETER AMBIGUITY

INTERFEROMETER AMBIGUITY

One of the problems normally associated with the use of multi-wavelength interferometers* is the requirement to resolve the 2π ambiguity associated with the relative phase measurements. Frequently this problem is resolved by the addition of appropriately placed additional receiver(s) along the baseline. However, for a low-orbiting interferometer receiving multiple transmissions spaced throughout the overpass, these ambiguity resolving receivers can be shown to be unnecessary. This is accomplished by means of an example.

Assume an interferometer to be in a circular polar orbit with the baseline parallel to the satellite's velocity vector. If at the point wherein the satellite's sub-point was zero degrees latitude and longitude a tramsmission from a platform was received and the relative phase measured was 0^{o}, then a baseline of multiple rf wavelengths might create (for example) the seventeen ambiguous lines-of-position (LOP) upon one of which the platform must lie as shown in Figure A.1.** While these LOP's are shown as distinct lines, their actual position is statistical in nature due to known noise corruption of the relative phase measurement as well as other system errors.

---

*For the systems described in the body of this report, this is not a problem due to the availability of doppler measurements for ambiguity resolution.

**These LOP's actually continue (mirror image) to the left of the satellite's north-south sub-track as well. However, this left-right ambiquity requires consideration of earth spin effects for its resolution.

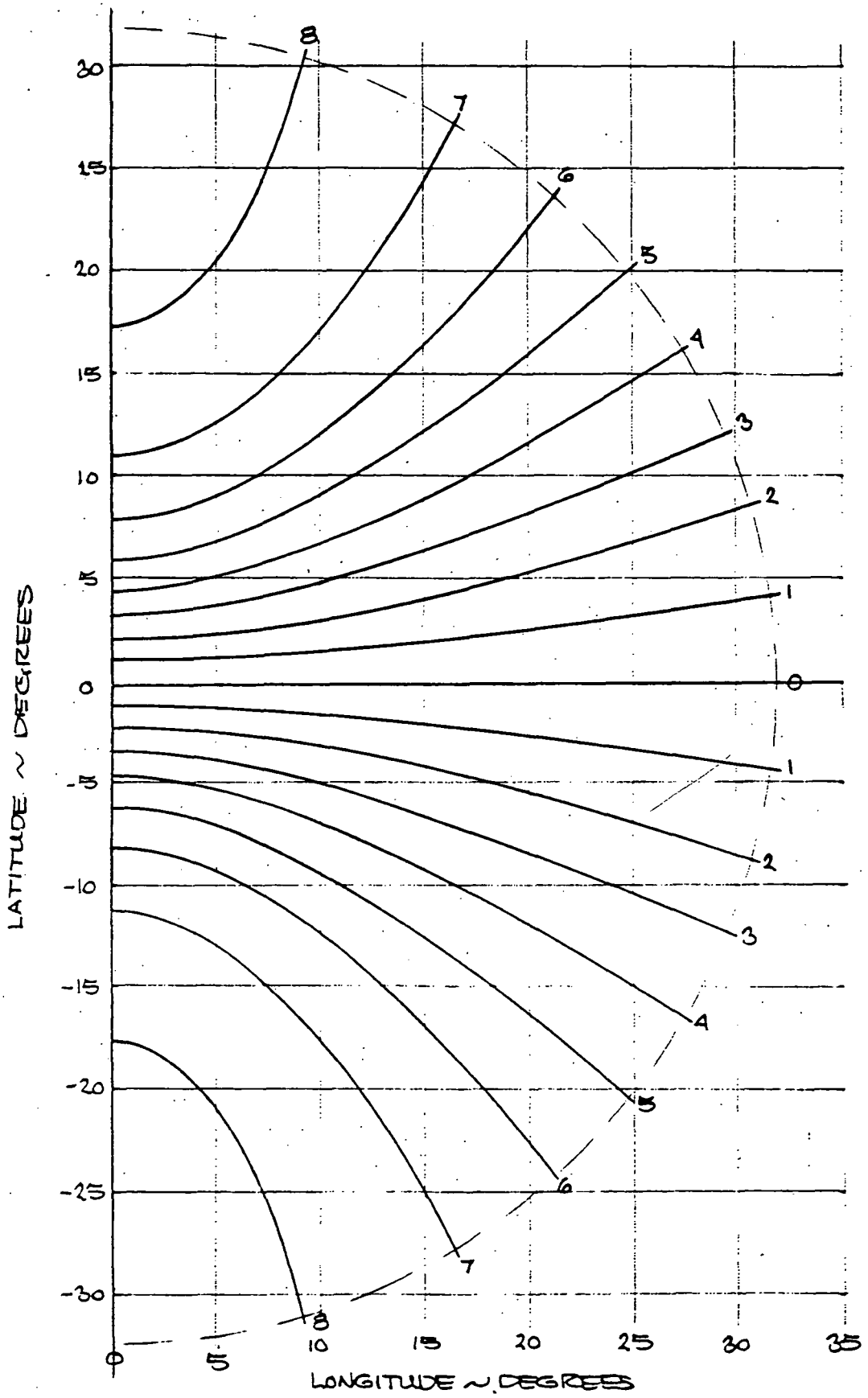

FIGURE A.1. AMBIGUOUS LINES OF POSITION

Therefore, the LOP's as shown might be considered to be "expected values" about which parallel LOP's exist which represent plus or minus potential statistical deviation.

With the LOP's from the first tramsmission fixed to the earth's surface, assume a second transmission is received from the platform when the satellite's sub-point is at 5^{o} north latitude. If again, the measured relative phase from this transmission was 0^{o}, then another set of LOP's identical to the first in shape and orientation relative to the satellite's sub-point could be fixed to the earth's surface and again the platform must lie on one of the seventeen LOP's. However, intersection of the first set of LOP's with the second set now indicate specific, individual latitudes and longitudes at which the platform could lie. These possible locations are indicated by the circles of Figure A.2 on the appropriate LOP derived from the first transmission.

While the intersections of Figure A.2 are denoted by circles, a better representation of these intersections would be ellipses whose major and minor axes as well as orientation are derived from intersection geometry and the noise/error characteristics of the system. This can be seen from the following sketch.

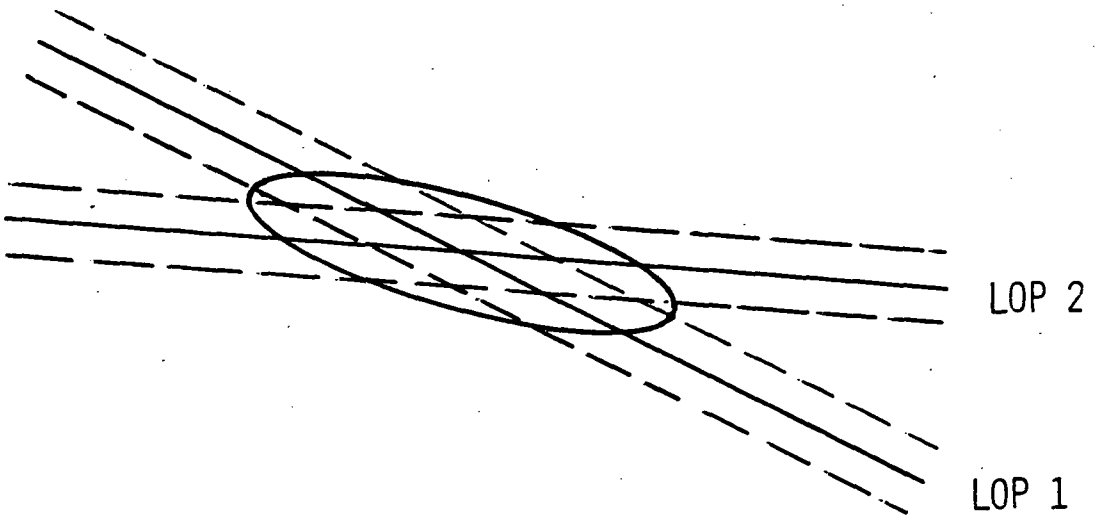

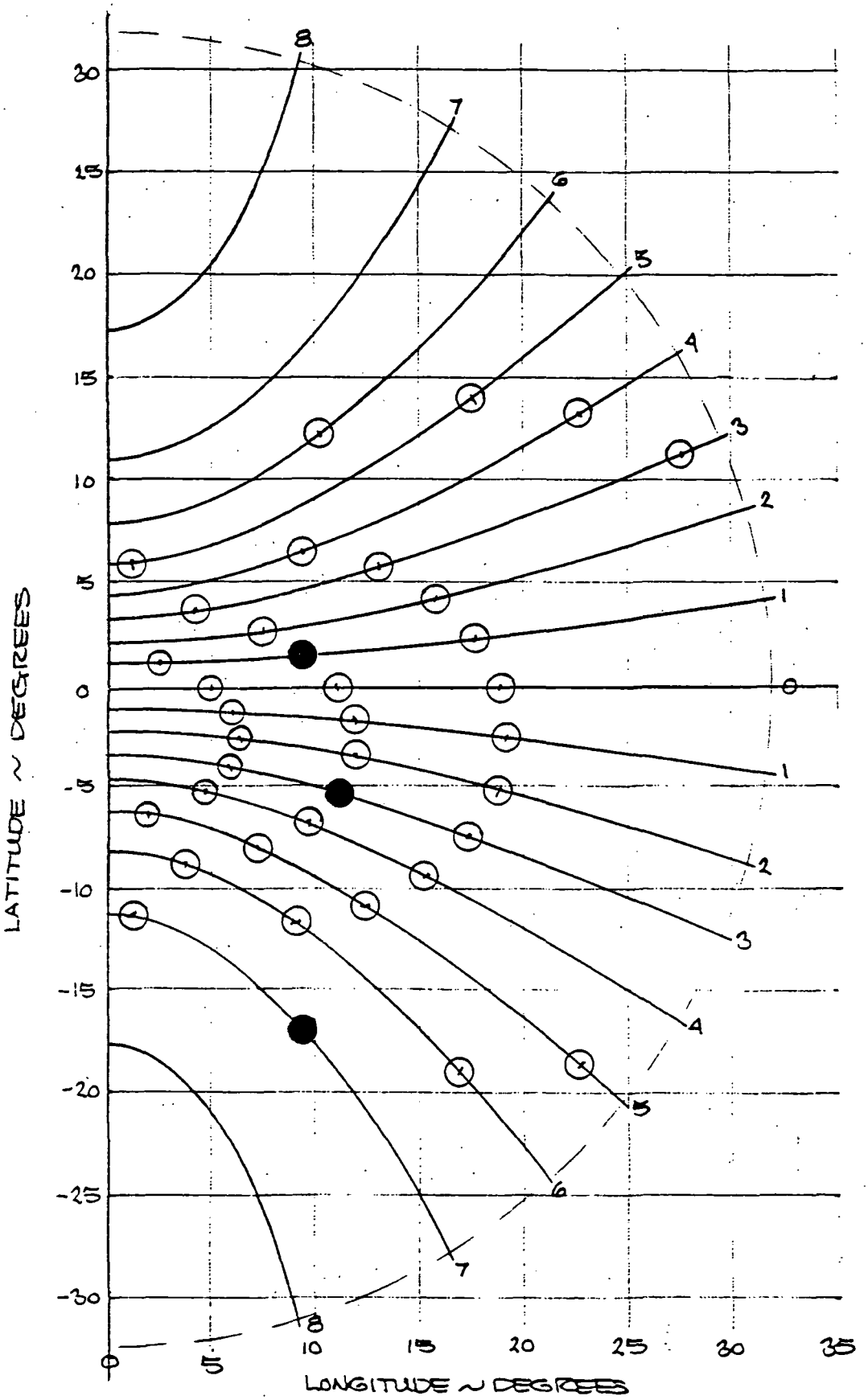

FIGURE A.2. POSSIBLE PLATFORM LOCATIONS AFTER TWO TRANSMISSIONS

The "expected value" position of the two LOP are indicated by the solid lines and represent (unless known biases exist) the measured relative phase. The dashed lines parallel to the LOP's represent (for example) no displacements of the LOP's based upon estimates of system errors. If a distribution for random errors can be assumed (e.g., normal), then areas within which the platform would lie with specified probability (neglecting ambiguity) can be established. This is indicated by the ellipse in the sketch above which would result from normally distributed errors.*

The receipt of the second platform transmission results in the thirty-seven possible locations for the platform shown in Figure A.2. Ambiguity resolving receivers would permit selection of one of these possible locations as the correct one. However, receipt of a third platform transmission and measurement of a relative phase again of zero, eliminates all but three of the thirty-seven ambiguous locations as being a potential location for the platform for the case where relative phase measurements are allowed to be in error by as much as $\pm 30^{o}$.** These three possible locations are indicated by the darkened circles of Figure A.2. A fourth transmission would resolve the ambiguity among these three, but analysis will show that the relative phase of the fourth transmission (satellite at 15^{o} north latitude) cannot possibly be zero degrees as the first three were assumed to be unless a greater error tolerance were assumed.

Based upon this example, the ambiguity resolution of a low orbiting interferometer should not require additional receivers for that purpose onboard the satellite. Although a more general investigation of orbit geometry, transmission repetition rate, and system errors is warranted, the present example indicates ambiguity resolution for a single axis interferometer can be accomplished with as few as three transmission receptions but probably no more than four. This same conclusion is equally applicable to multiple arm (e.g., cross-arm) interferometers although the number of required transmissions may only be two or three.

---

*Software implementation of this process would yield the covariance matrix for this intersection geometry provided the least-square technique were employed.

**For a lesser error tolerance, none of the thirty-seven ambiguous locations are possible - i.e., for the assumed conditions the measured relative phase of the third transmission cannot possibly be zero degrees.

APPENDIX B

SYSTEM DESCRIPTION

METEOROLOGICAL ADVANCED LOCATION AND DATA COLLECTION SYSTEM (MALDCS)

I. OVERVIEW

A major step in reducing the cost of satellite-borne data collection and location systems was taken during the 1970's with the advent of the RAMS and ARGOS systems. However, both systems burden data collection platforms with stringent stability specifications on reference oscillators. The ability to relax these specifications represents a substantial cost reduction opportunity for these systems. The Meteorological Advanced Location and Data Collection System (MALDCS) described here does not require highly stable oscillators, making possible truly low-cost platforms that are well-suited to mass deployment in global meteorological experiments.

The essential features of the system are depicted in Figure 1.1. Balloon-borne transmitters send periodic bursts that are received by the polar-orbiting satellite. Each transmission burst contains the identity of the balloon and meteorological data such as temperature and barometric pressure. Due to Doppler shift and the lack of synchronism between the platforms, the transmissions received by the satellite are random in both frequency and time. At the satellite, the presence of the signals are detected, identification and data messages are demodulated, the signal RF frequency is measured relative to a local reference, and the relative phase between two separated antennas is measured. These data along with the time of signal reception are transmitted in real time to ground processing facilities, or are recorded for later transmission. The frequency and phase measurements are used to determine position and velocity through a combination of Doppler and RF interferometer estimation algorithms.

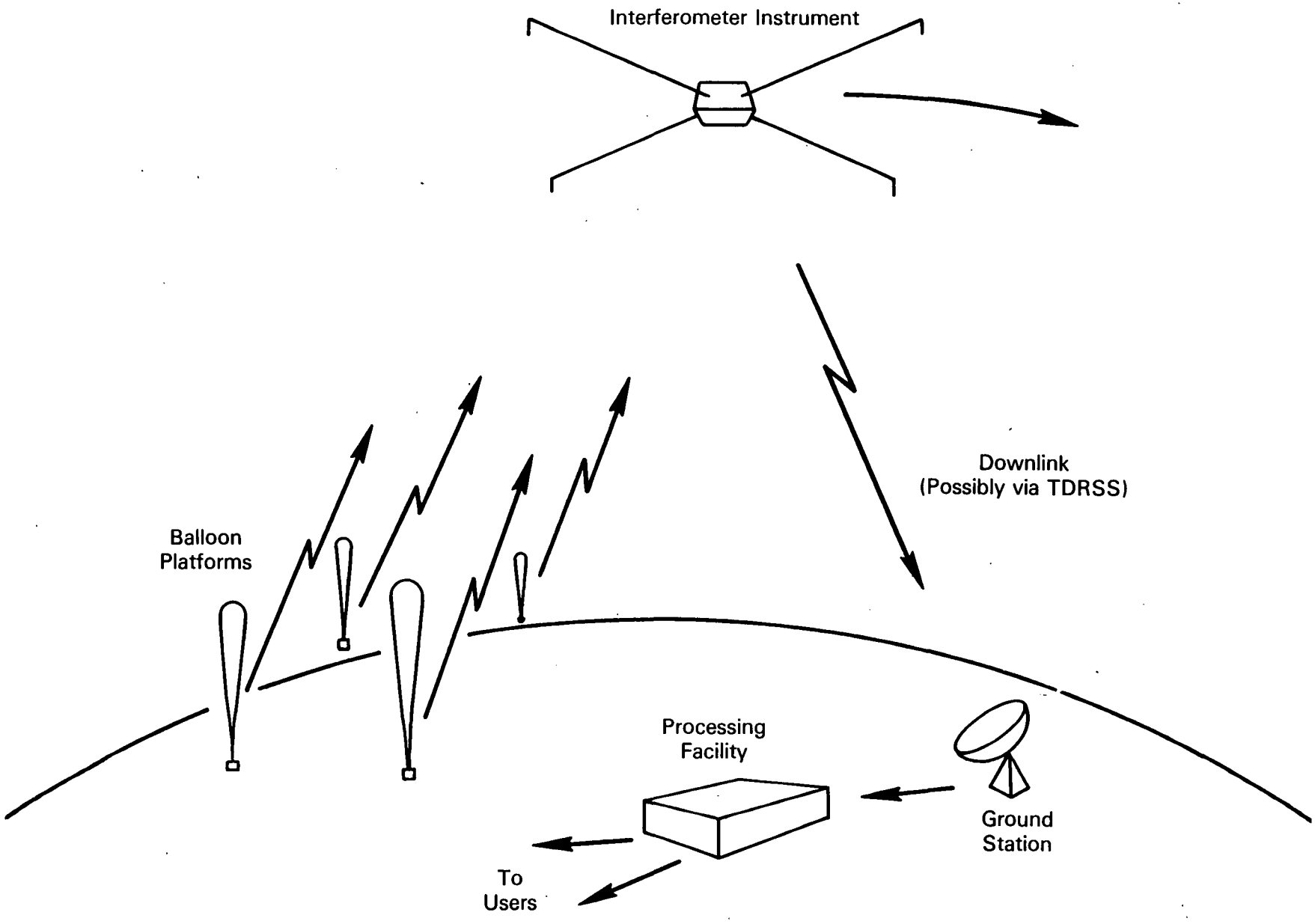

FIGURE 1.1. MALDCS SYSTEM CONCEPT

The space segment of the MALDCS utilizes advanced techniques for rapid signal detection and frequency estimation. When a transmission is detected, a phase-lock loop is commanded to tune to it. After the loop acquires the signal, data demodulation, Doppler frequency measurement, and interferometer phase difference measurements all proceed simultaneously. This allows short transmission bursts and a low bit rate, minimizing time and frequency interference between the random bursts.

The space segment uses four antennas, arranged on two orthogonal interferometer baselines. The baselines are oriented at 45° with respect to the satellite's velocity vector. This geometry results in a near-optimum location error distribution when Doppler and interferometer data are used in combination.

The reduction in platform oscillator stability requirements is achieved through newly developed algorithms for processing the frequency measurements. RAMS and ARGOS specifications limit the frequency change during an overpass to a few Hertz. The new algorithms, on the other hand, are capable of compensating for any linear drift of oscillator frequency during the overpass, so that the drift does not contaminate Doppler data. Interferometer data is inherently immune to oscillator drift.

II. SYSTEM CHARACTERISTICS AND PERFORMANCE

The salient characteristics and performance parameters of the system are summarized below.

- Orbit: Sun-synchronous, 830 km altitude
- Candidate spacecraft: TIROS-N with modified[1] altitude control system
- Antennas: four, quadrifilar helix, shaped beam
- Antenna Baselines[2]: two, oriented $\pm 45^{o}$ with respect to spacecraft velocity vector, 25 meters long
- Boom Type[3]: Continuous longeron Astromast fiberglass, pretwisted
- Location estimation error: 1 km max
- Velocity estimation error, single overpass[2]: 1.5 m/s max
- Probability of reception of a single platform transmission, N platforms in view: 1 - 0.02N
- Bit error rate: 10^{-4}
- Number of data bits per transmission: 42

- Maximum total number of active platforms[4]: 4000
- Platform bit rate: 200 b/s
- Platform transmission period: 60 s
- Platform transmission length: 0.36 s
- Platform transmission modulation[5]: smoothed phase modulation, Manchester signalling, 50^{o} peak
- Transmitted platform power[5]: 1 W
- Platform oscillator frequency range: 401 MHz 16 kHz
- Platform oscillator drift: linear drift allowed during satellite overpass

Notes:

1. See Section 3.3 of report body for modifications required.

2. Baseline length optimized for minimum velocity estimation error, based on dynamic and thermal boom excursion estimate. See Figure 5.5 of report body.

3. See Section 2.1 of report body for boom description.

4. Number of active platforms limited by 12-bit address.

5. Modulation and link analysis in ORI TR 1864.

III. SYSTEM CONFIGURATION AND OPERATION

3.1 BALLOON PLATFORMS

The balloon platforms contain instruments for making meteorological measurements, a microprocessor-based data acquisition and control unit, and an RF transmitter.

The instruments carried are a thermometer, barometer, hygrometer, and possibly a radar altimeter. Each instrument's reading is sampled once per minute and the samples are encoded into binary digits which are impressed onto the RF carrier along with a platform identification code. The range and resolution of the instruments determines the number of bits required to transmit the readings. The assignment is as follows:

Instrument	Range	Resolution	Bits
Thermometer	-65 to 35^{o}C	0.1^{o}C	10
Barometer	50-1050 mb	0.25 mb	12
Hygrometer	0-100% RH	0.1%	10
Altimeter	0-20 km	30 m	10

The data acquisition and control unit assembles the data bits from the instruments and adds the 12 bit platform address and the synchronization patterns to form the complete platform message, which is 70 bits long.

At regular one-minute intervals, the control unit triggers the RF transmitter on, and reads the platform message, at a rate of 200 b/s, into the modulator. When all the message bits have been sent, the transmitter is turned off until the next transmission. There is a delay of 25 ms between turning on the transmitter and starting the modulation, to allow the receiver time to acquire the signal. The total length of the transmission is 360 ms.

The transmitter consists of an oscillator, modulator, and power amplifier. The oscillator is an inexpensive crystal-controlled unit that is well-insulated to insure that ambient temperature transients are "smoothed out" before they are felt by the crystal. This smoothing is necessary so that any frequency variation during the satellite overpass appear to be approximately linear with time. Linear frequency variations have minimal impact on the accuracy of the position and velocity estimation algorithm used.

The modulation technique used is akin to minimum-shift keying (MSK) in that the phase varies linearly in time. This produces spectral sidebands that decrease rapidly with distance from the carrier, minimizing adjacent-signal interference. In addition, Manchester signalling is used so that the signal includes an isolated carrier component from which the modulation sidebands are easily filtered. This enables the interferometer receivers to measure the signal phase difference during the entire transmission.

The low bit rate makes it possible to use digital waveform synthesis to generate the modulated signal. With this method, a digital version of the desired waveform is read from memory into a digital-to-analog converter, the output of which drives the phase modulator. Alternately, the desired RF waveform could be constructed with some low carrier frequency, by digital synthesis, and then this signal could be upconverted to the transmit frequency. Because of the low relative cost of complex digital components and their inherent stability, use of such techniques would probably result in lower cost and better performance compared with standard analog methods.

3.2 FLIGHT INSTRUMENT

The MALDCS flight instrument may be carried aboard a satellite similar to the TIROS-N, in a polar orbit of about 830 km altitude. The instrument uses four antennas, one at the end of each of two orthogonal baselines. The two baselines are oriented at a 45 angle with respect to the spacecraft velocity vector, and in a plane perpendicular to the spacecraft yaw axis. The two antennas on a baseline are held a distance of 25 m apart by two booms of about 12 m each. The booms are 10-inch diameter Astromasts with continuous fiberglass longerons.

The antennas are a circularly polarized quadrifilar helix design, approximately one meter in length and 7.5 cm in diameter. Their receive pattern is circularly symmetrical about the axis, and has a gain that increases, to a point, with off-nadir angle. This compensates partly for the increase in platform range corresponding to increasing off-nadir angle.

Figure 3.1 is a partial block diagram of the flight instrument, showing the antennas of one of the baselines. Each platform transmission is received by both antennas simultaneously. The two versions of the signal are amplified, filtered, and translated to an IF frequency. The IF signals are distributed to each of five tunable data extraction units, each of which consists of a phase detector, a frequency counter, and a demodulator. The IF signal from one of the antennas is also supplied to a signal detection unit. This unit determines the frequency of platform transmissions when they begin, and sends a tuning command to one of the data extraction units. This data extraction unit locks onto the signal, measures its phase and frequency, and demodulates it to extract the digital data. The phase and frequency measured is sent along with the platform identification and data to the spacecraft data handling subsystem.

The equipment configuration associated with the pair of antennas connected to the second baseline is similar to that shown in the block diagram, but the data extraction units consist of phase detectors only, and there is no signal detection unit. The data extraction units associated with the second baseline are tuned by the same commands as those of the first.

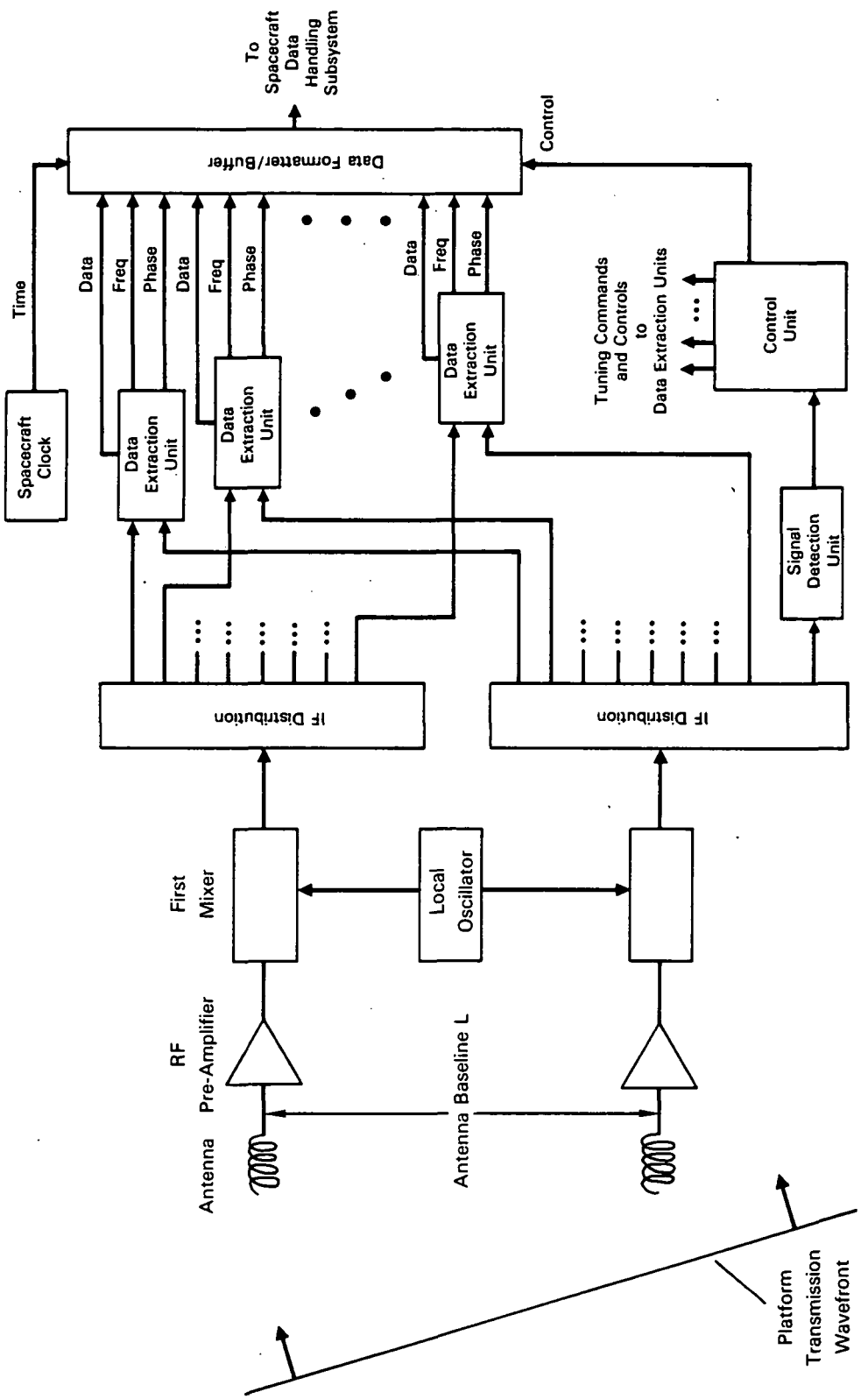

FIGURE 3.1. MALDCS FLIGHT INSTRUMENT BLOCK DIAGRAM

The interferometer is periodically calibrated by injecting calibration signals into the RF inputs. The signals are of the same form as the platform transmissions, but are of a known, fixed, phase and frequency. The calibration signals are processed, and their data sent to the ground, in the same way as the platform transmissions. They are recognized during ground processing and used to generate corrections in the position and velocity estimation computations. In addition to this on-board calibration, the system is calibrated periodically using ground-based platforms at known locations.

3.3 PLATFORM POSITION AND VELOCITY ESTIMATION

Three independent measurements are made of each platform transmission: the difference in signal phase across the two interferometer baselines, and the signal frequency, from which the Doppler frequency is determined. At least ten transmissions are received from a platform during the satellite overpass that most closely approaches it. The resulting thirty data points are used, along with the time of receipt and the satellite ephemerides, to determine an estimate of platform position at a specified time, and velocity averaged over the overpass duration. The platform oscillator and drift rate are also estimated in the process.

Each Doppler frequency measurement locates the platform somewhere on a line-of-position (LOP) that is symmetrical about the spacecraft velocity vector. This LOP is the intersection of a cone with the velocity vector as its axis, and the Earth's surface. (The platform is assumed here to be on the surface for simplicity.) The Doppler measurement determines the apex angle of the cone. An interferometer phase difference locates the platform on one of a family of LOPs, each one of which is the intersection of the surface and a cone having the interferometer baseline as its axis. The phase measurement determines the family of apex angles of the cones. The number of LOPs in the family is equal to the number of wavelengths in the baseline. For the 25m baseline at 400 MHz, there are 32 LOPs. The Doppler data combined with the interferometer data from one baseline yields a family of points at which the platform could be located. These points are the intersections of the Doppler LOP and the 32 interferometer LOPs.

The second interferometer baseline of system likewise gives a family of LOPs for each platform signal phase measurement. Since the interferometer axes are orthogonal, this set of LOPs will be rotated with respect to the other by 90°. As with the other interferometer baseline, the combination of the phase measurement and the Doppler measurement gives a family of points on the surface corresponding to possible platform positions. If there were no measurement errors, the intersection of the two families of points would be a single point, the actual location. In practice, measurement errors combine to make the exact location of the LOPs, and their intersections, uncertain. Considering the errors, the intersection of the families of points may include more than one pair that are close enough to coincidence to constitute a highly probably location. However, this ambiguity is easily resolved by using the data from the other transmissions during the overpass. Two or three transmissions is normally sufficient to make an unambiguous position estimate.

The intersection of the uncertain LOPs can be viewed as a two-dimensional probability density. The shape of the contours of the density depends greatly on the angle of intersection of the LOPs. The optimum contour shape is a circle, because it corresponds to a location error that is independent of direction. If the contour were an ellipse, on the other hand, it would mean that errors in one direction (along the major axis) are larger than those in other directions. The contour shapes can only be made circular near nadir. They always become more and more elliptical as one moves away from nadir, and geometric dilution of precision (GDOP) effects increase. In a combined Doppler/cross-arm interferometer system, one obtains location errors that are (as nearly as possible) direction independent by orienting the inteferometer baselines symmetrically at angles with respect to the velocity vector. The optimum angle is dependent on the relative magnitude of the Doppler and interferometer errors. The 45° configuration used represents a near-optimum arrangement with equal errors.

Figure 3.2 shows the consequences of orienting the interferometer axes at 45 with respect to the velocity vector. The figure shows three superimposed families of LOPs. The family that is symmetrical about the vertical shows several of the possible LOPs that would be given by the Doppler measurement. The families of curves that are symmetrical about the ± 45°

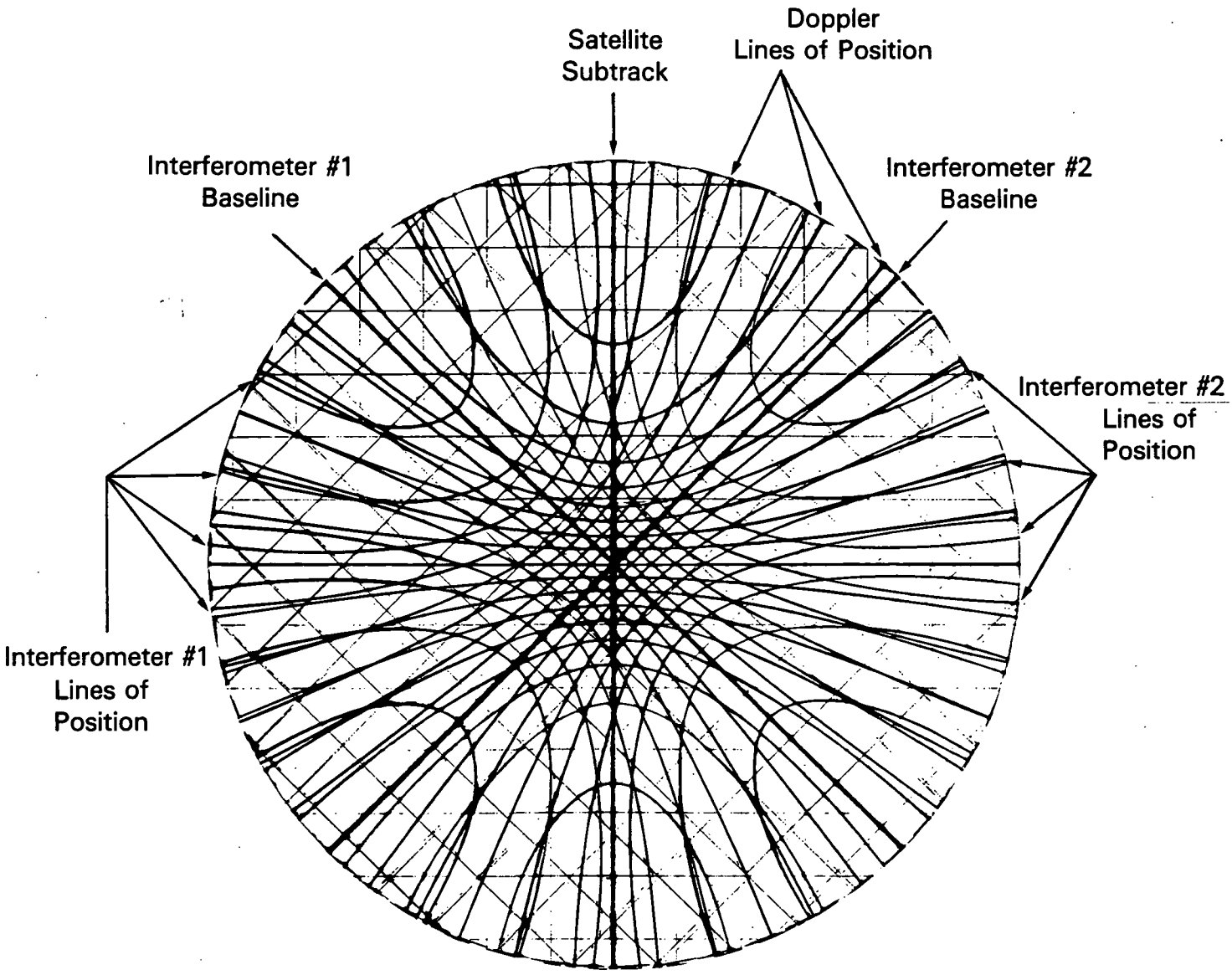

FIGURE 3.2. SUPERPOSITION OF LINES OF POSITION FROM DOPPLER AND TWO INTERFEROMETER BASELINES AT $\pm 45^{o}$

lines represent LOPs that are given by interferometer phase measurements when the baselines are oriented at ± 45°. It is seen that the LOP intersection geometry near nadir is almost circularly symmetrical, which corresponds to direction independent errors.

ORI, Inc.
1400 Spring Street, Silver Spring, Maryland 20910
(301) 588-6180